~~CONFIDENTIAL~~

AN ANALYTICAL METHOD FOR PREDICTING LIFT AND DRAG CHARACTERISTICS OF FLAT-TOP WING-BODY COMBINATIONS AT SUPERSONIC SPEEDS

by

Dennis F. Hasson

Thesis submitted to the Graduate Faculty of the

Virginia Polytechnic Institute

in candidacy for the degree of

MASTER OF SCIENCE

in

Aeronautical Engineering

APPROVED:

Director of Graduate Studies

APPROVED:

Head of Department

Dean of Engineering

Major Professor

May 1958

Blacksburg, Virginia

~~CONFIDENTIAL~~

TABLE OF CONTENTS

PAGE

I. LIST OF FIGURES AND TABLES

FIGURE PAGE

II. INTRODUCTION

One of the most important problems associated with airplanes flying in the supersonic flight regime is the achievement of adequate range capabilities. (Range is defined as the distance from a base to an objective, and a return to the base.) Range is evaluated from the classic Brequet range equation, and is dependent on several parameters. The most important parameter from an aerodynamic standpoint is the lift-drag ratio which is a measure of the efficiency of the aerodynamic design. The aerodynamic design of an airplane, therefore, should be directed toward obtaining a high value of maximum lift-drag ratio.

In the design of supersonic airplanes it is found that more volume is required for items such as the crew, fuel, powerplant, payload, etc., than is available in the wings of the airframe which must be thin to attain supersonic speeds. In order to provide the required volume, a fuselage (body) would be used to house the above items. The only criteria governing the size and shape of this body would be that it provide the required volume with a minimum penalty in drag. The possibility of developing a significant amount of lift from this body is in general not considered.

As one might expect, however, the interference between the body and the wing at supersonic speeds will have a large influence on the aerodynamic characteristics. The present design trend is towards lower wing aspect ratios and lower wing span to body diameter ratios. The interference lift between the body and the wing can become, therefore,

significant, if the body is arranged properly such that it will induce lift on the wing (ref. 1). It would be of interest, therefore, to investigate configurations of this type which would accomplish this.

One of the initial investigations was made by Eggers and Syvertson in reference 2. They attacked the problem by considering an elementary theory which they called the "momentum principle". The principle stated that the components of an aircraft should individually and collectively be arranged to impart the maximum downward and the minimum forward momentum to the surrounding air. They set down requirements to meet such practical considerations as aerodynamic heating, structural weight, and stability problems with the objective of obtaining high maximum lift-drag ratios. It was reasoned that this could be accomplished with an expanding body (e.g., a cone) mounted beneath a sonic-leading-edge wing with their apexes being coincident. This configuration, then would fulfill all of the above requirements, and would result in high values of maximum lift-drag ratio at supersonic speeds. The investigators named their configurations "flat-top wing-body combinations," and this notation is used throughout the text. The configuration utilized the positive pressure field of the body on itself and on the undersurface of the wing to provide the configuration with a significant amount of interference lift at zero angle of attack necessary to provide a lift coefficient equal to the lift coefficient for maximum lift-drag ratio of the wing. Consequently, the lift-drag ratios of the configurations might approach the high values associated with the wing-alone values. The results of the experimental investigation, which included a study of wing planform and tip deflection,

yielded high values of maximum lift-drag ratio, approximately 6, through a Mach number range from 3 to 6.28. These results were very encouraging.

The above exploratory experimental investigation, however, was somewhat limited in scope. The experimental investigation was extended in reference 3 to cover several additional shape variables such as fuselage fineness ratio, fuselage profile shape, wing-leading-edge sweep, and the additional of auxiliary bodies. For conical fuselages, increases in the cone angle at Mach numbers of 3 to 4.2 gave some increase in maximum lift-drag ratio, while at the high Mach numbers of 5 to 6.28 a more slender fuselage was more favorable. The best profile shape seemed to be the 3/4-power body. The effect of leading edge sweep on the maximum lift-drag ratio was dependent on the free-stream Mach number and fuselage shape. Addition of auxiliary bodies increased not only the lift but also the drag, resulting in a reduced lift-drag ratios. The highest lift-drag ratio obtained was 7.2 at a Mach number of 3.00 with a semiconical body mounted beneath an arrow wing. This paper, then, provided an experimental approach for determining some of the important parameters governing the optimization of the configurations proposed by Eggers and Syvertson.

While most of the bodies in the foregoing investigations had circular cross sections, Jorgensen proposed that the bodies should be of elliptic cross section. He noted that the pressure drag of a cone, of given length and base area, decreases as the cross section is changed from circular to flat (major axis in the angle-of-attack plane), and that the theory predicts the elliptic cone produces larger gains in lift and lift-drag ratio

pared to circular cones. This original investigation (ref. 4) was for winged-circular and elliptical cones, and the results showed the elliptic cone configurations to be somewhat superior. Jorgensen extended his work (ref. 5) to obtain data on elliptical semicones mounted beneath arrow wings as in the previous two investigations. Also included in this investigation was the effect on the maximum lift-drag ratio of increasing the volume by adding additional volume to the base of the model. The results did not show any favorable increases in maximum lift-drag ratio for the elliptical semicones mounted beneath arrow wings. The best value measured was 7.3 at a Mach number of 2.94. One of the more interesting results obtained was that the maximum lift-drag ratio increases as the volume parameter $\frac{(\text{Body volume})^{2/3}}{\text{plan area}}$ decreases.

All these investigations indicated that the flat-top wing-body combinations are efficient aerodynamic configurations. The high values of maximum lift-drag ratio obtained seem to indicate that they might be a solution to the problem of providing maximum range capability at supersonic speeds.

At present, however, the analytical work has not been as extensive as the experimental investigations mentioned above. One of the papers which has been published (ref. 6) gives a very good treatment of the problem of theoretically predicting the maximum lift-drag ratios of flat-top configurations and assesses the efficiency with which the interference lift is utilized. A number of calculations, using the linear theory, were made to determine the influence of body lift conditions on the

aerodynamic characteristics of these configurations, along with an assessment of the accuracy of the linear theory. The analysis - which included full-conical bodies, and half-conical bodies mounted above and below the wing - showed that the most efficient configuration was the one proposed by Eggers, namely, the flat-top configuration. This analysis, however, did not take into account such items as viscous forces and the wave drag (thickness drag) of a finite wing. The results, therefore, were useful only in determining the best of three configurations studied, and the general aerodynamic trends. Thus, a more detailed treatment of the problem was needed which includes the above neglected terms.

Such a treatment is given by Migotsky and Adams in reference 7. They analyzed two types of configurations which might effectively utilize the pressure field around a body of revolution. The configurations investigated were a half-cone and semi-Newtonian ogive mounted under a thin sonic-leading-edge triangular wing. The lift induced on the wings by the half-cone was calculated at zero angle of attack by means of the Kopal tables (ref. 8). The wave drag of the wings was evaluated using the linear theory, and the interference effects between wing and body, when the configuration is at angle of attack, were also estimated from the linear theory. The skin-friction drag for the Mach number range from 1.5 to 5.0 was estimated using the Karman-Schoenherr theory and an appropriate ratio of the compressible to incompressible skin-friction coefficient.

The above analysis, however, was restricted to triangular wings mounted above a semi-cone, and a semi-Newtonian ogive. In the present paper the methods of Migotsky and Adams (ref. 7) are used for predicting the lift

and drag characteristics of two additional flat-top wing-body combinations. These are a semiconical body mounted beneath an arrow planform wing and a 3/4-power semibody mounted beneath a diamond planform wing, and these configurations are known as arrow wing and diamond wing configurations, respectively, throughout the remainder of the text. Slightly different methods from those used in reference 7 are employed for obtaining the individual terms which contribute to the lift and drag of the flat-top configurations. The author considers these methods to be more applicable to the problem considered in the present analysis. The results of the analysis are compared with experimental tests performed at a Mach number of 3.35 in order to obtain a check on the analysis. This Mach number is significant, because it is the Mach number at which the body bow shock is coincident with the wing leading edge for the configurations considered.

III. SYMBOLS

A aspect ratio, $\frac{b^2}{S}$

A_b area of base, sq ft

$A' = \beta A$

a local speed of sound, ft/sec

a_0 speed of sound at any arbitrary location and time, ft/sec

b wing span, ft

C_D drag coefficient

C_D' drag coefficient, $\frac{\text{Drag}}{qS}$ (zero base drag)

C_{D_b} base drag coefficient, $\frac{\text{Base drag}}{qS}$

C_{D_f} skin friction drag coefficient, $\frac{c_f W_s}{S}$

C_L lift coefficient, $\frac{\text{Lift}}{qS}$

C_{L_α} lift-curve slope, per radian

C_p pressure coefficient, $\frac{p - p_\infty}{q_\infty}$

$\bar{c}$ wing chord, ft

c_f average skin friction coefficient

G see appendix C (eq. (C9))

H stagnation pressure, lb/sq ft

$K_1 = n\beta$

k constant of proportionality

L/D lift-drag ratio, $\frac{C_L}{C_D}$

M Mach number

$m' = \beta \cot \gamma$

$n = \frac{\tan \gamma}{\tan \mu} = \frac{K_1}{\beta}$

$n_1 = \frac{\tan \gamma}{\beta}$

$n' = \frac{\tan X}{\beta}$

p static pressure, lb/sq ft

q dynamic pressure, $\frac{\bar{\gamma}}{2} pM^2$, lb/sq ft

R free-stream Reynolds number based on M.A.C.

r_b radius of base, ft

S wing planform area, sq/ft

$s = \frac{\tan \sigma}{\tan \gamma}$

$s' = \frac{\cot \sigma}{\cot \gamma}$

$\frac{t}{c}$ airfoil thickness-chord ratio

u,v,w perturbation velocity components, ft/sec

V total velocity, ft/sec

W_s wetted area, sq/ft

X sweep of shock angle, deg; ($\tan X = \cot \gamma$ for sonic leading edge)

x,r cylindrical coordinates in a meridian plane

x,y,z Cartesian coordinates

Σ summation of

α angle of attack, deg

$\beta = \sqrt{M_\infty^2 - 1}$

γ leading-edge sweep angle, deg

$\bar{\gamma}$ ratio of specific heats, 1.405 for air

θ direction of flow at a point, deg

λ taper ratio, $\frac{\text{Tip chord}}{\text{Root chord}}$

$$\bar{\lambda}_i = \frac{z - z_i}{\frac{t}{c}\left(x - x_i\right)}$$

$$\Delta\bar{\lambda}_i = \bar{\lambda}_i - \bar{\lambda}_{i-1}$$

μ Mach angle, $\sin^{-1}\frac{1}{M}$

σ trailing-edge sweep angle (positive for sweepback), deg

ϕ perturbation (small disturbance) velocity potential

Subscripts:

B body

B_p body pressure

max maximum

n value at any point

o conditions at zero angle of attack

S stability axes

s conditions at shock

W wing

W_w wing wave

∞ conditions in free stream

IV. ANALYSIS

An analysis for determining the lift and drag characteristics of flat-top wing-body combinations is presented. The analysis will be general enough in nature to apply to any desired wing planform or body contour. Some details of the analysis presented herein, however, will only be applicable to the two configurations considered.

The particular configurations analyzed consisted of a semiconical body mounted beneath a biconvex section arrow planform wing and a 3/4 power $\left(r = kx^{3/4}\right)$ semibody mounted beneath a modified biconvex-section diamond planform wing.

Throughout the analysis the following assumptions are made, unless otherwise noted:

1. The leading edge of the wing is coincident or ahead of the body shock (sonic leading edge or supersonic, respectively).

2. The base drag is zero; that is, the pressure on the base of the configuration is equal to the free-stream static pressure.

3. The linear theory is applicable; that is, the fluid is considered to be homogeneous, and nonviscous (except where the skin friction was treated separately), and the disturbance perturbances were small enough so that their squares and products were considered negligible when compared with the square of the stream velocity.

The derivation of the lift and drag relations as functions of the angle of attack is made in two parts; namely, the zero angle-of-attack case, and the angle-of-attack condition. Further breakdowns result for

two reasons: namely, (1) the individual terms which contribute to the lift and drag are treated separately; and (2) differences in the two configurations considered. It is to be noted that all coefficients throughout the analysis are based on the total wing area. The zero angle-of-attack case is considered first.

ZERO ANGLE OF ATTACK

The zero angle of attack is defined as the angle at which the wing reference line and the supersonic free stream are alined. The individual lift and drag terms which result will be introduced separately. First to be considered is the body pressure drag and lift, and the lift induced on the wing by the body. The following discussion will describe how these quantities arise and how to evaluate them.

Consider a body of revolution of finite length in a uniform supersonic flow (see Fig. 1(a)). Pressures are felt on the surface of the body and positive pressures are produced in the field due to the presence of the body in the flow field. The pressures acting on the surface contour produce a drag force. Since the pressures at every point around the periphery of any cross section are equal, as indicated in section A-A, no resultant lift is produced. However, if the body is cut in half by the X-Y plane and the upper half removed (Fig. 1(b)), the drag of the body is decreased by a half and a resultant lift force on the body occurs. Further, if we bound the pressure field caused by the body (bounded by the body surface and the shock) with a solid surface in the X-Y plane, we

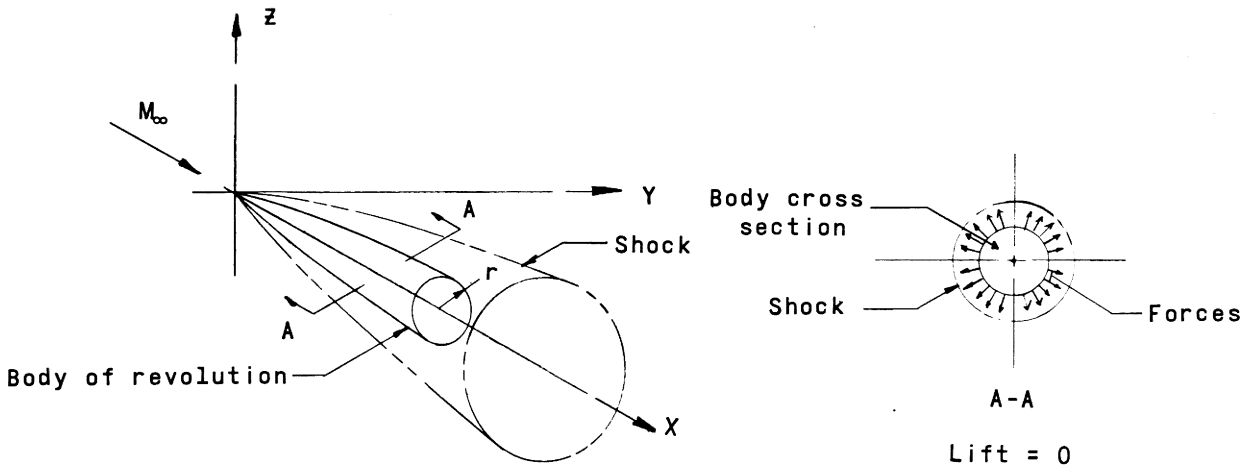

(a) Body of revolution in a supersonic stream.

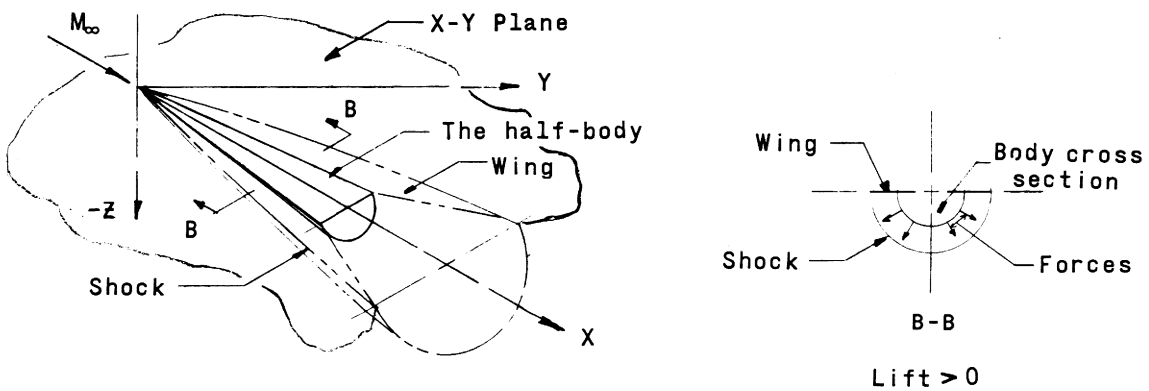

(b) Half body of revolution bounded by X-Y plane.

Figure 1.- Sketch of the flow field about a body of revolution in a supersonic stream.

preserve these pressures and impart them to the surface (see Fig. 1(b)). This produces an induced lift due to the presence of the body. This surface could, of course, be a wing. Theoretically the wing would have its leading edge coincident with the shock (since the presence of the body is not felt in the free stream), and would extend in the positive x-direction to infinity. However, practical considerations dictate a finite planform. Such a planform is shown in Figure 1(b).

A solution for the flow field about the body of revolution must be obtained in order to evaluate the forces mentioned above. One such solution is the exact method of characteristics. This method was used for the present analysis. An outline of the method of characteristics and its application to the solution of the flow field about a body of revolution is given in appendix A. The method of characteristics yields the physical properties of the flow, and thus provides the information necessary to calculate the pressure coefficient at any point behind the shock and on the body surface. To illustrate this we first consider the expression for the linear pressure coefficient in a supersonic stream. The expression is

$$C_p = \frac{2}{\gamma M_\infty^2}\left(\frac{p}{p_\infty} - 1\right) \tag{1}$$

where

$$\frac{p}{p_\infty} = \frac{p}{H_\infty}\frac{H_\infty}{p_s}\frac{p_s}{p_\infty} \tag{2}$$

and where

p static pressure at any point behind the shock

H_∞ stagnation pressure in the free stream

p_s static pressure at the shock

p_∞ static pressure in the free stream

Now, to obtain the pressure coefficient along the rays in the conical flow field at the nose, the ratios of equation (2) can be replaced by the following relations

$$\left.\begin{aligned} \frac{p}{H_\infty} &= (1 - V^2)^{\frac{\bar{\gamma}}{\bar{\gamma}-1}} \\ \frac{p_s}{H_\infty} &= \left(1 - V_s^2\right)^{\frac{\bar{\gamma}}{\bar{\gamma}-1}} \\ \frac{p_s}{p_\infty} &= \frac{2\bar{\gamma}}{\bar{\gamma}+1}\left(M_\infty^2 \sin^2 X - \frac{\bar{\gamma}-1}{2\bar{\gamma}}\right) \end{aligned}\right\} \qquad (3)$$

where

X shock angle

V total velocity at any point behind the shock

V_s the velocity at the shock.

Note: V and V_s are equal to the square root of the sum of the squares of their tangential and radial velocity components.

Thus, the pressure coefficient along any ray in the conical field is

$$C_p = \frac{2(\bar{\gamma}-1)}{(\bar{\gamma}+1)}\left[\frac{2\sin^2 X}{\bar{\gamma}-1} - \frac{1}{\bar{\gamma}M_\infty^2}\right]\left[\frac{1 - V^2}{1 - V_s^2}\right]^{\frac{\bar{\gamma}}{\bar{\gamma}-1}} - \frac{2}{\bar{\gamma}M_\infty^2} \qquad (4)$$

For all other points beyond the cone, in the net and on the body surface, the ratios in equation (2) are evaluated by making use of velocities and pressure relations at these points. The pressure coefficient, equation (1), is then computed for all these points. The method of determining the body pressure drag and lift and lift induced by the body on the wing from these pressure coefficients is presented next.

In order to illustrate how the body pressure drag and lift coefficient and body induced lift on the wing were computed, a sketch of a typical body and its net are shown in Figure 2. From the figure we see that the body pressure drag and lift coefficient are given by the following expressions:

a. Body pressure drag coefficient

$$C_{D,B_p} = \frac{\pi}{2S} \sum_{1}^{n} C_{p,n}\left(r_n^2 - r_{n-1}^2\right) \tag{5}$$

b. Body lift coefficient

$$C_{Lo,B} = \frac{2}{S} \sum_{1}^{n} C_{p,n}\left(A_n - A_{n-1}\right) \tag{6}$$

where the A's are areas between points along the body center line bounded by the body contour.

The computation for the lift induced on the wing included the lift in the conical field, and the lift in the net with the shock and the trailing edge as boundaries. The wing was considered to be a flat plate

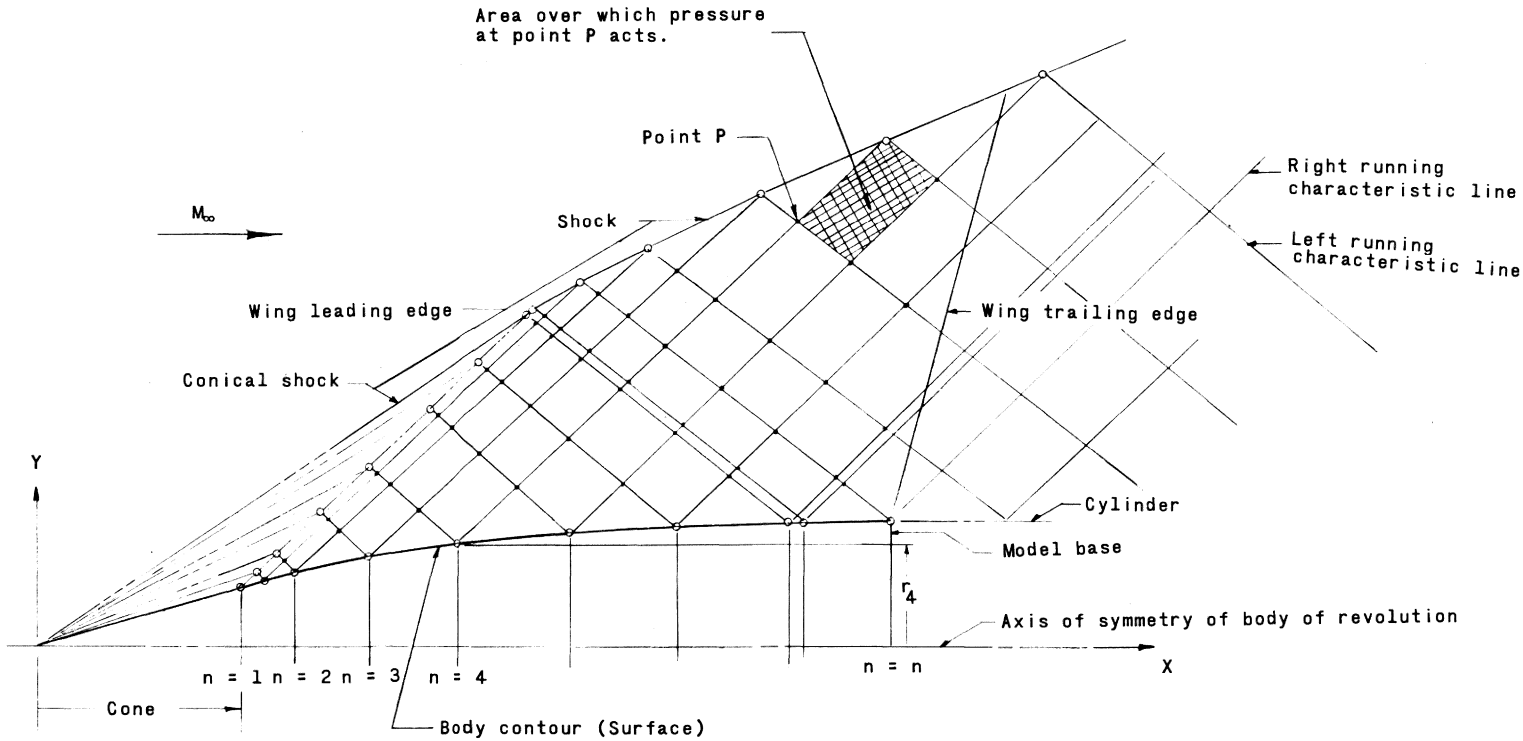

Figure 2.- Typical characteristic net about a body of revolution in a supersonic stream.

for these computations. The lift coefficient was evaluated by adding the results of the separate terms which were evaluated as follows:

1. Lift-coefficient of conical field is given by the product of the pressure coefficient along a ray times the area below the ray (starting with the first ray beyond the cone and ending with the shock) summed over the area between the body surface and the shock divided by half of the total wing area.

2. Lift-coefficient in the net is given by the product of the pressure coefficient at the intersection of two characteristics times the adjacent area (e.g., the shaded area adjacent to point P in Fig. 2) summed over the area enclosed by the body contour, the up going characteristic lines of the conical field, and the wing trailing edge divided by half of the total wing area.

Since the wings tested experimentally have finite thickness, there is a pressure drag associated with their thickness. This drag is called the wave drag. The problem of evaluating the wave drag of wing sections other than the diamond is somewhat difficult. The general method for solution of the fundamental linearized equations for pressure drag at supersonic speeds consists of solving the disturbance velocity potential due to a sheet of constant strength sources distributed over the wing planform and imposing the boundary condition that the flow must be parallel to the airfoil at the surface. A difficulty, however arises, when the continuous curvature of the airfoil surface (such as the biconvex sections tested in this paper) makes the integration of the potential

equations extremely difficult. This difficulty was overcome in reference 9 by approximately the biconvex profile (or any curved profile) by a multisided polygon and obtaining the drag-coefficient solution by superimposing the known solution for single triangles of constant slope. The resulting drag relation using this analysis is

$$-\beta \frac{C_D}{\left(\frac{t}{c}\right)^2} = \sum_{i=1}^{n} \sum_{j=i+1}^{n} C_{ij} \, \Delta\bar{\lambda}_j \, \Delta\bar{\lambda}_i \tag{7}$$

where the coefficient C_{ij} is dependent on:

N the number of equally spaced straight line segments per surface used to approximate the airfoil

$$\frac{K_{N+1}}{K_1} = \frac{\tan \sigma}{\tan \gamma}$$

$$n_1 = \frac{\tan \gamma}{\beta}$$

This solution is subject to the restriction that the airfoil section be the same at all spanwise stations, and that the boundary conditions imposed on the wing are satisfied in a horizontal plane rather than on the actual airfoil surface. It is obvious that the above expression is somewhat difficult to evaluate as it stands. Grant and Cooper, however, in reference 10 presented tables for the rapid evaluation of this equation for sweptback wings of arbitrary section with both subsonic and supersonic leading edges with supersonic trailing edges. The wave drag of the wings presented in the present analysis were evaluated using the results of this reference. The specific values for wing wave drag of

the particular wings considered herein were determined from Figures 3(a) and 3(b). In these figures the variation of the wave drag parameter $\frac{\beta C_D}{4\left(\frac{t}{c}\right)^2}$ with the ratio of the tangent of the leading edge sweep angle to β for three values of the ratio of tangent of the trailing edge to the tangent of the leading edge are presented for the 5-percent biconvex section, and 3-percent modified biconvex section. These calculations were based on dividing the chord into twenty equal parts resulting in a 20 sided polygon which approximated the airfoil section. It was found in reference 10 that this was a sufficient number for negligible error.

In order to account for viscous effects, skin friction on the surface is considered. In the evaluation of the skin-friction drag it was assumed that the boundary layer was turbulent over the entire configuration. Although a number of theories exists for predicting the average skin friction coefficient, the Frankl-Voishel Extended Theory of reference 11 was used. This theory has the restrictions of a linear variation of viscosity with temperature, and an insulated surface (zero heat transfer at the surface). These restrictions do not seem to limit the applicability of the theory to this paper, since the Mach number and temperature considered are not high. The average skin friction coefficient is given by the following interpolation formula which represents results computed numerically to within ±2 percent in the range $0 < M_\infty < 4$:

$$c_f = \frac{0.472}{\left(\log_{10} R\right)^{2.58}\left(1 + \frac{\bar{\gamma} - 1}{2} M_\infty^2\right)^{0.467}} \qquad (8)$$

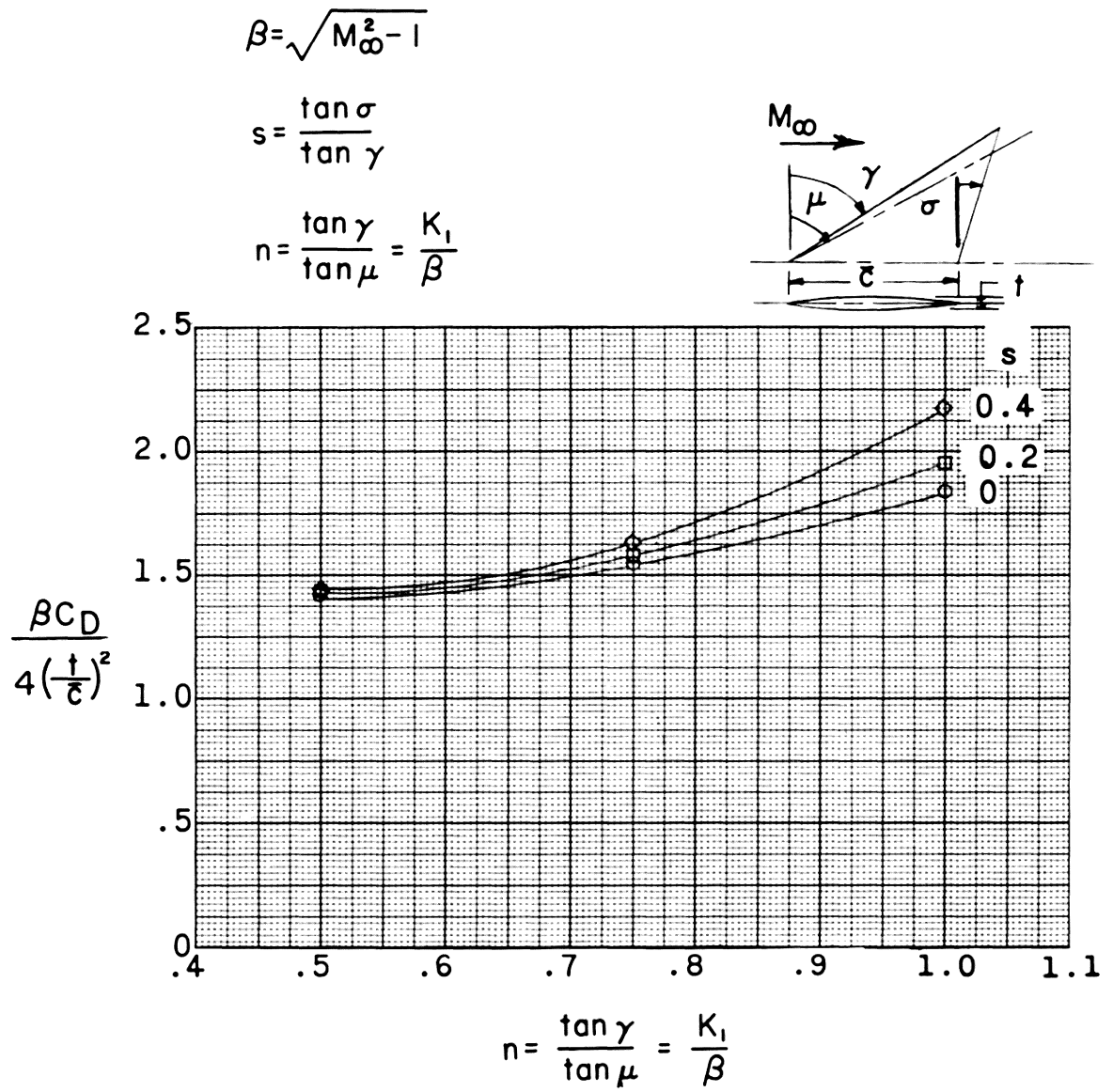

(a) 5 percent biconvex arrow wings.

Figure 3.- Variation of the wave drag parameter $\frac{\beta C_D}{4\left(\frac{t}{\bar{c}}\right)^2}$ with the leading edge sweep parameter, $n = \frac{\tan\gamma}{\beta}$.

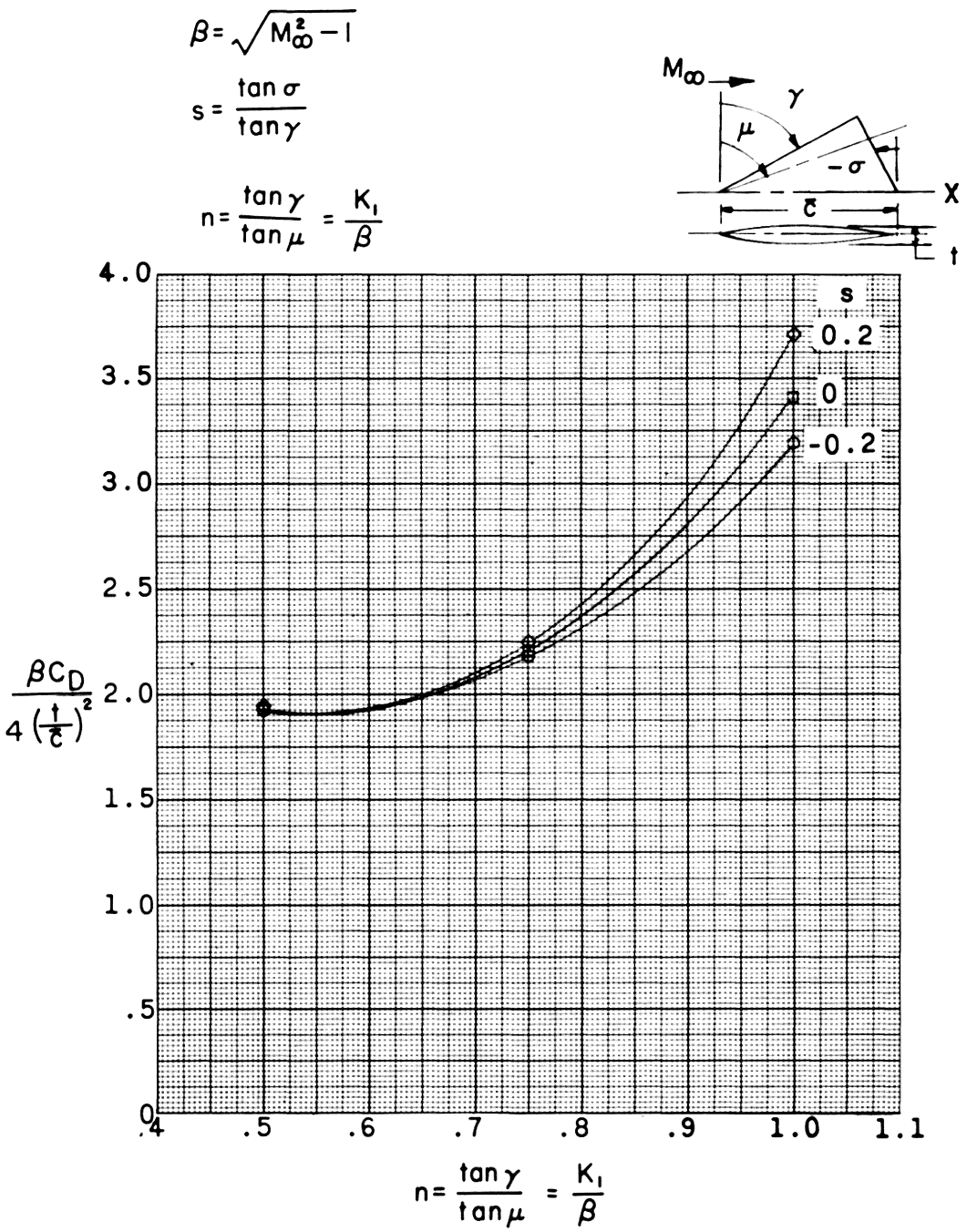

(b) 3 percent modified biconvex diamond wings. (Coordinates for $0 < x < 0.05\bar{c}$ were not considered.)

Figure 3.- Concluded.

The skin-friction drag coefficient is therefore $C_{D_f} = \frac{c_f W_s}{S}$ where W_s is the total wetted area.

The total drag at zero angle of attack is then obtained from the sum of the body pressure drag, the wing wave drag, and the skin friction drag. This result is written symbolically in the following equation.

$$C_{D_o} = C_{D,B_p} + C_{D,W_w} + C_{D_f} \tag{9}$$

Due to the complexity of the equations and since the wing is considered to be very thin, no attempt has been made, in the present investigation, to compute the interference drag of the wing flow field on the body, or the body flow field on the curved under-surface of the wing.

ANGLE OF ATTACK CONDITION

For the angle of attack condition it is assumed that the pressures due to angle of attack may be obtained from linear theory for the wing alone and that these additional pressures can be superimposed on the pressures obtained at zero angle of attack. It is further assumed that the angle of attack is sufficiently small so that second and higher order terms in α may be neglected, the lift coefficient is written as

$$C_L = C_{L_o} + C_{L_\alpha} \alpha \tag{10}$$

where

C_{L_o} sum of the body lift and body induced lift on the wing at zero angle of attack

C_{L_α} lift-curve slope $\left(\frac{\Delta C_L}{\Delta \alpha} \text{ at } \alpha \approx 0^\circ\right)$, per radian

α angle of attack, radians

It is observed that the lift, as given above, for any angle of attack other than zero, is being carried completely by the wing planform.

The lift-curve slopes for the arrow and diamond wings were evaluated from the formulas in reference 12. The scope of this reference is limited to wings of vanishingly small thickness with no camber and is valid only for wings with supersonic leading and trailing edges, i.e., the component of the free stream velocity normal to the leading and trailing edges is supersonic. The geometric characteristics of the wings considered in the analysis met these restrictions except that they have finite thickness. Within the order of the approximation, however, this violation is not sufficient to invalidate the results. An outline of the determination of the equation of lift-curve slope and a summary of the conditions to be satisfied for the particular formula used are given in appendix B.

Utilizing the same assumptions made in the above discussion the drag coefficient may be written

$$C_D' = C_{L_\alpha}\alpha^2 + C_{L_O}\alpha + G\alpha + C_{D_O} \tag{11}$$

The first linear term, $C_{L_O}\alpha$, results from the zero-lift pressures acting on the slopes due to angle of attack. The other linear term, $G\alpha$, results from the angle of attack pressures on the zero angle of attack slopes. The contribution to the latter term resulting from the flat

plate angle of attack pressures acting on the upper surface of the wing was considered negligible. The quantity G, therefore, includes only the effect of the angle of attack pressure field of the wing acting on the surface of the body, and was evaluated by assuming that the angle of attack pressure acting on the body was constant over the body and equal to the pressure at the root chord (along the wing center line) of the wing. The quantity G is derived in appendix C for the case of a sonic leading edge, and the equation is written as

$$G = \frac{2r_b^2}{S} \frac{\tan \gamma}{\sqrt{\beta^2 \tan^2 \gamma - 1}} \cos^{-1}\left(\frac{1}{\beta \tan \gamma}\right) \qquad (12)$$

The values of the various terms used in equations (10) and (11) for the two configurations are presented in Table I. The expressions (10) and (11) define the lift and drag relations with angle of attack for flat-top wing-body combinations. It is left to obtain an experimental check on the accuracy of these relations. This is accomplished in the next part of the text.

TABLE I.- SUMMARY OF THE VALUES OF THE VARIOUS TERMS USED IN THE LIFT AND DRAG EQUATIONS

Item	Values for -	
	Semiconical body with arrow wing	3/4-power semibody with diamond wing
C_{D,B_p}	0.0070	0.0022
C_{D,W_w}	0.0055	0.0028
C_{D_f}	0.0053	0.0048
$C_{L_o,B}$	0.0280	0.0102
$C_{L_o,W}$	0.0308	0.0215
C_{L_α}, per radian	1.3514	1.2247
G	0.042651	0.022364

V. EXPERIMENTAL TESTS

In order to obtain an experimental verification of the theoretical predictions made in the analysis, wind tunnel tests were performed on two models. The selection of the models and test Mach number was based only on satisfying as closely as possible the assumptions in the analysis. The models were of the flat-top type with the body and wing apexes being coincident.

MODELS

The models, as mentioned above, were selected solely to satisfy as closely as possibly, the assumptions of the analysis. The wing leading-edge sweep, therefore, was chosen to be equal to the sweep of body shock at a particular Mach number (for this investigation a Mach number of 3.35) to insure a sonic leading edge. Also, thin wing sections were chosen so as not to exceed the limitations of the linear theory. To illustrate the applicability of the analysis to flat-top wing-body combinations, two configurations were chosen which differed both in body contour and wing planform.

The first model consisted of a semiconical body mounted beneath an arrow planform wing. The wing had a 5-percent biconvex section, 70.35° of leading edge sweep, and an aspect ratio of 2.0. Photographs and a three view drawing are presented in Figures 4 and 5, respectively.

The other model consisted of a 3/4 power, $r = kx^{3/4}$, semibody mounted beneath a diamond planform wing. The wing had a 3-percent section (modified NACA 65A series for 0 to 50 percent of the chord, and biconvex from

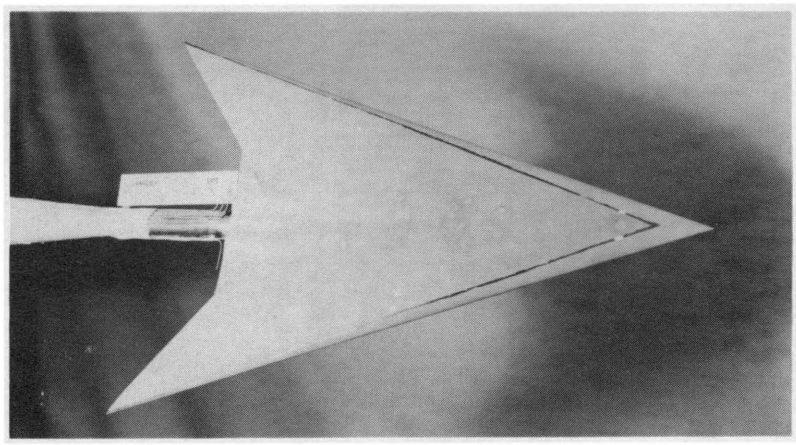

Plan view

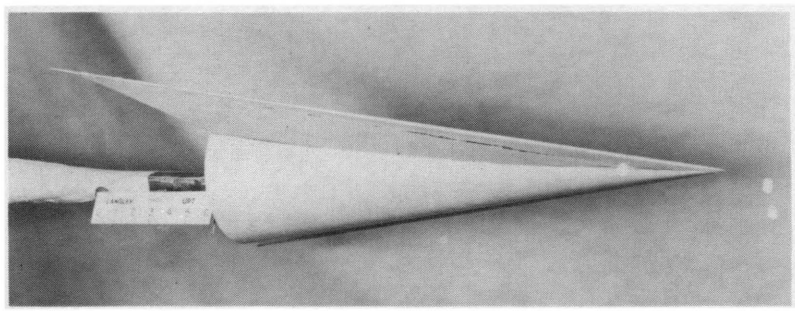

Side view

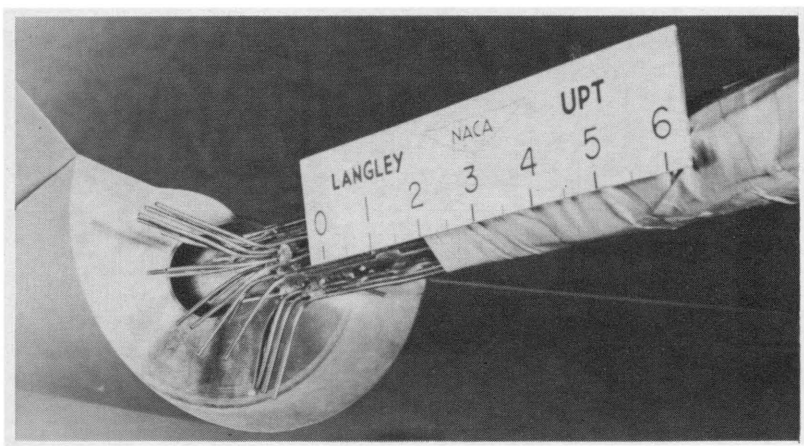

Rear view

Figure 4.- Photographs of the arrow wing configuration. L-58-1622

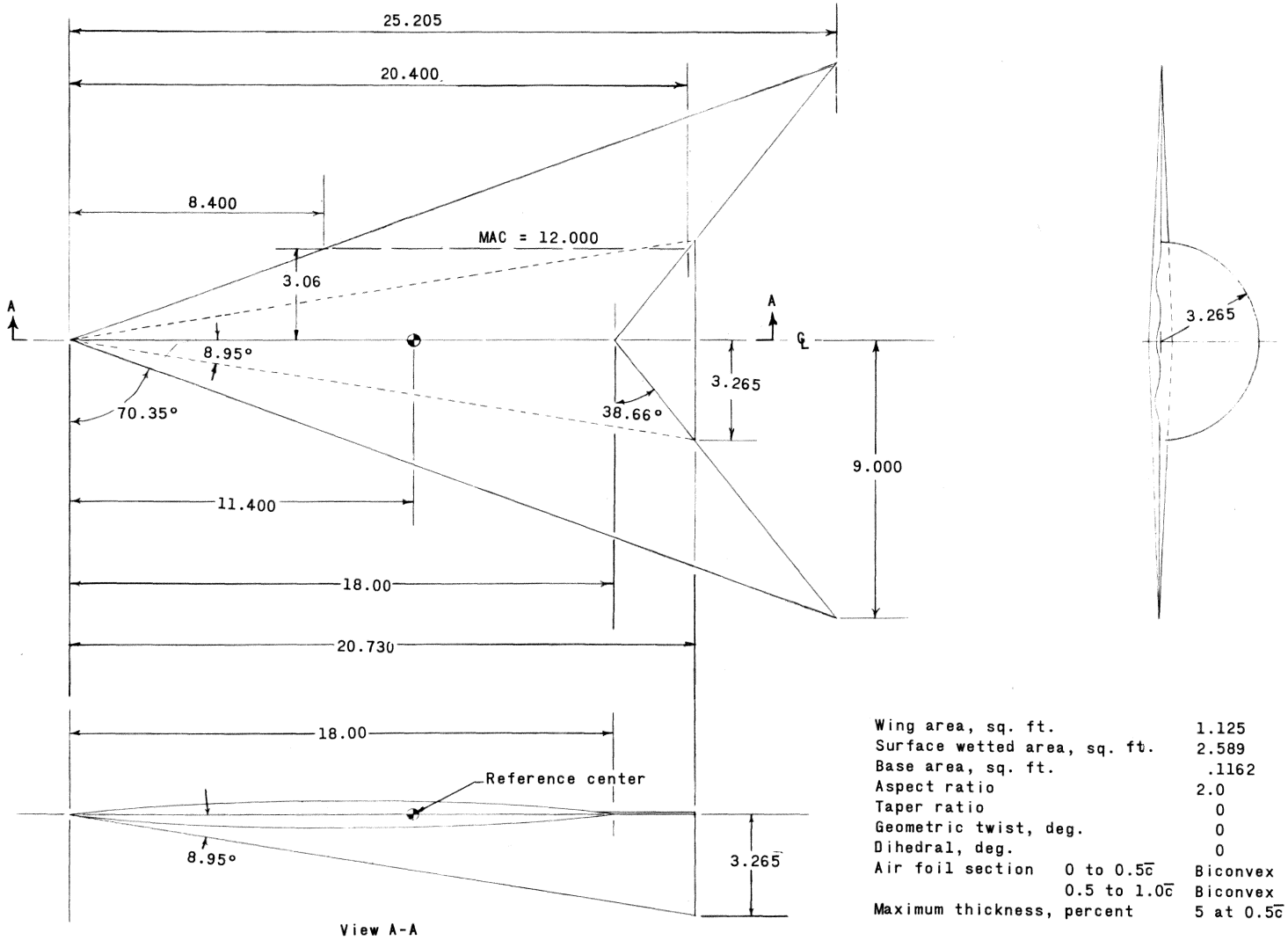

Wing area, sq. ft.		1.125
Surface wetted area, sq. ft.		2.589
Base area, sq. ft.		.1162
Aspect ratio		2.0
Taper ratio		0
Geometric twist, deg.		0
Dihedral, deg.		0
Air foil section	0 to 0.5$\bar{c}$	Biconvex
	0.5 to 1.0$\bar{c}$	Biconvex
Maximum thickness, percent		5 at 0.5$\bar{c}$

Figure 5.- Three-view drawing of the arrow wing configuration. Dimensions are in inches unless otherwise noted.

50 to 100 percent), 70.3° of leading edge sweep, and an aspect ratio of 1.3. Photographs of the model and a three-view drawing are presented in Figures 6 and 7, respectively. A table of the wing ordinates is presented in Table II.

WIND TUNNEL

The tests were made in the high-speed test section of the Langley Unitary Plan wind tunnel. The working section is 4 feet high and 4 feet wide and approximately 7 feet long. Some details are presented in Figure 8. The operating Mach number range for this test section is 2.3 to 4.65.

The basic elements of the complete facility are shown schematically in Figure 9. They consist of a 100,000 horsepower compressor drive system, (compressor lineup) a dry air supply and evacuating system (auxiliary equipment and dry air storage), a cooling system (cooling tower), and the necessary interconnecting ducting to produce the proper air flow through either of the two test sections. Conditions in the tunnels are controlled at the main drive control panel. Data outputs from the model are recorded on the readout equipment located outside the test sections.

The test sections are of the closed type, and utilize an asymmetric, fixed geometry, variable Mach number nozzle. A variable Mach number nozzle is one which permits a variation of Mach number of any desired increment throughout its range with the tunnel operating. The design of such a nozzle is dependent on the method of characteristics and a typical

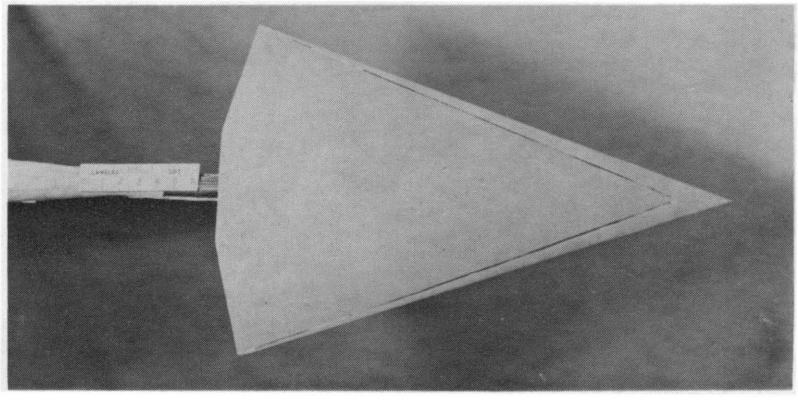

Plan view

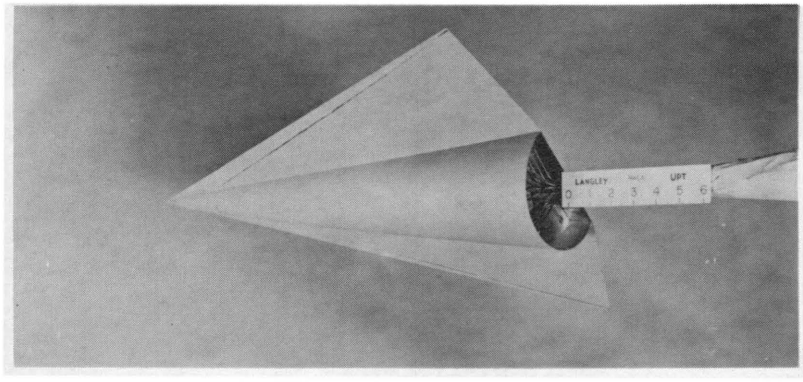

Side view

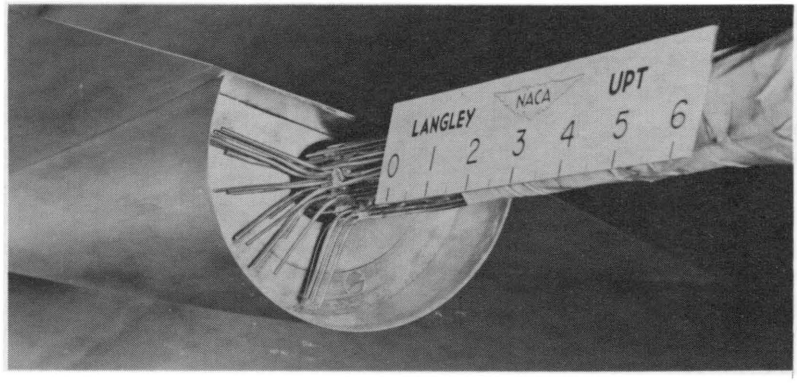

Rear view

Figure 6.- Photographs of the diamond wing configuration. L-58-1623

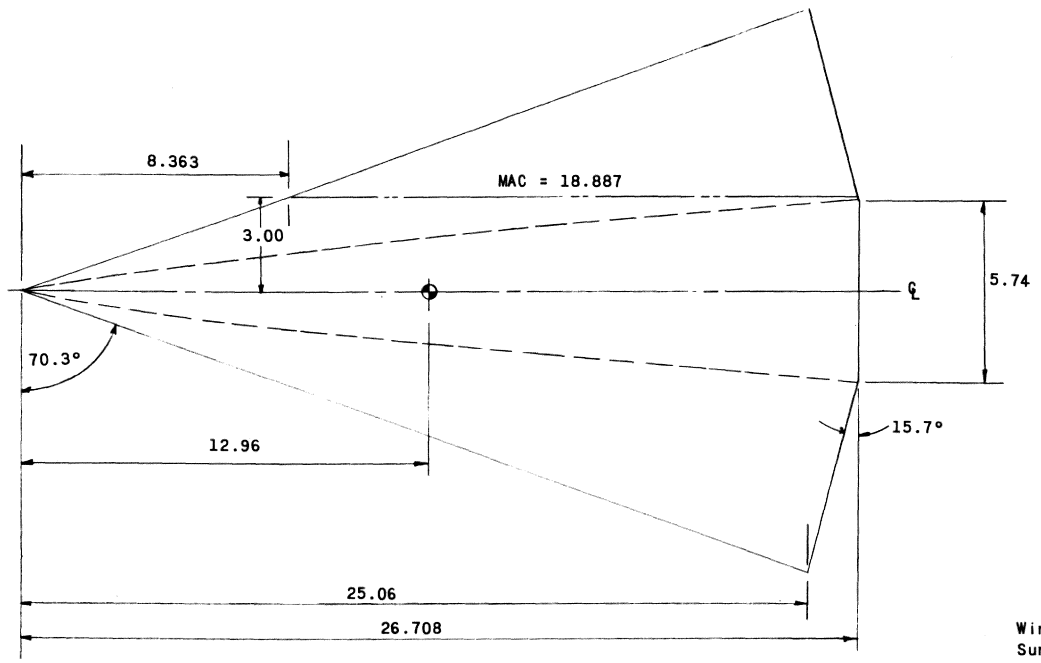

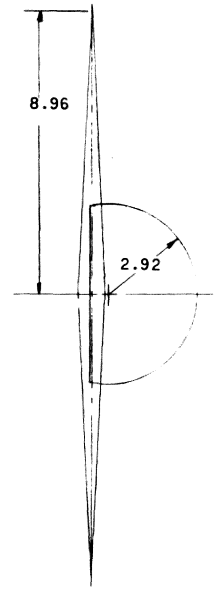

Wing area, sq. ft.		1.716
Surface wetted area, sq. ft.		3.814
Base area, sq. ft.		.1127
Aspect ratio		1.3
Taper ratio		0
Geometric twist, deg.		0
Dihedral, deg.		0
Air foil section	0 to 0.5$\bar{c}$	Mod.NACA 65 Series
0.5 to 1.0c	0.5 to 1.0$\bar{c}$	Biconvex
Maximum thickness, percent		3 at 0.5$\bar{c}$

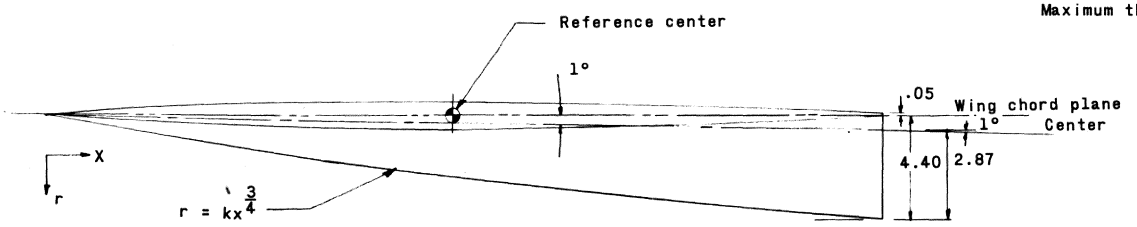

Figure 7.- Three-view drawing of the diamond wing configuration. Dimensions in inches unless otherwise noted.

TABLE II.- AIRFOIL COORDINATES FOR THE 3-PERCENT DIAMOND WING

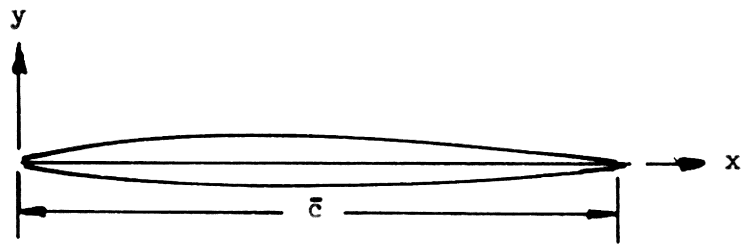

Modified NACA 65 series (0 to 0.5$\bar{c}$)	
x, percent $\bar{c}$	y, percent $\bar{c}$
0	0
.5	.2157
.75	.2563
1.25	.3299
2.5	.4327
5	.5964
10	.8414
15	1.0216
20	1.1523
25	1.2665
30	1.3515
35	1.4189
40	1.4657
45	1.4962
50	1.5

Biconvex (0.5$\bar{c}$ to 1.0$\bar{c}$)	
x, percent $\bar{c}$	y, percent $\bar{c}$
50	1.5
55	1.485
60	1.44
65	1.3653
70	1.2603
75	1.1258
80	.9605
85	.7659
90	.5405
95	.2853
100	0

CONFIDENTIAL

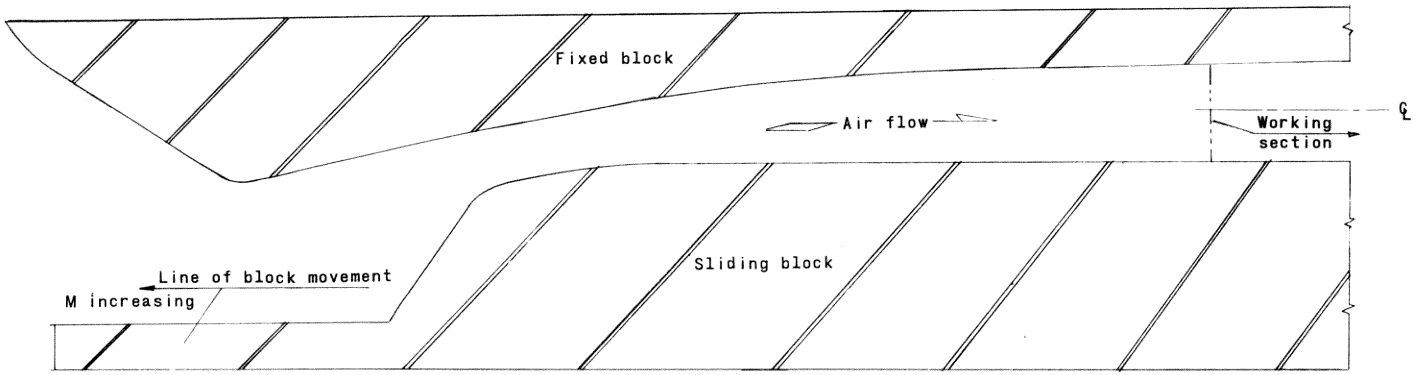

Typical cross section of an asymmetrical nozzle.

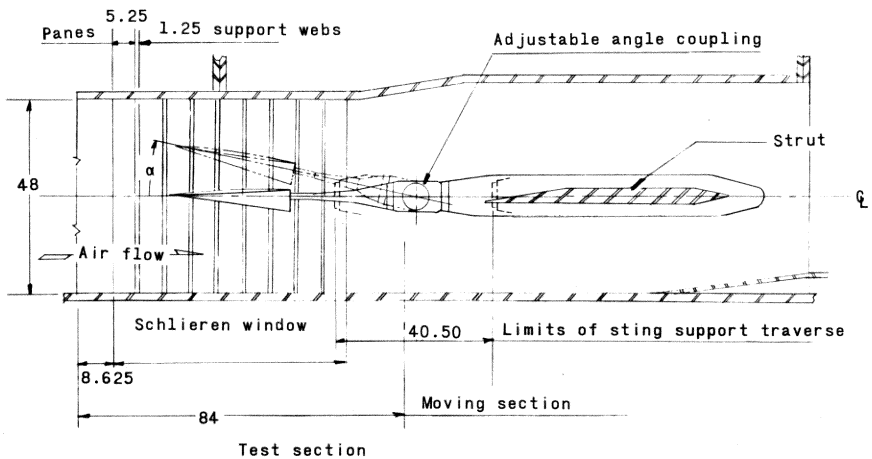

Figure 8.- Test section and a typical cross section of an asymmetric nozzle. Dimensions are in inches unless otherwise noted.

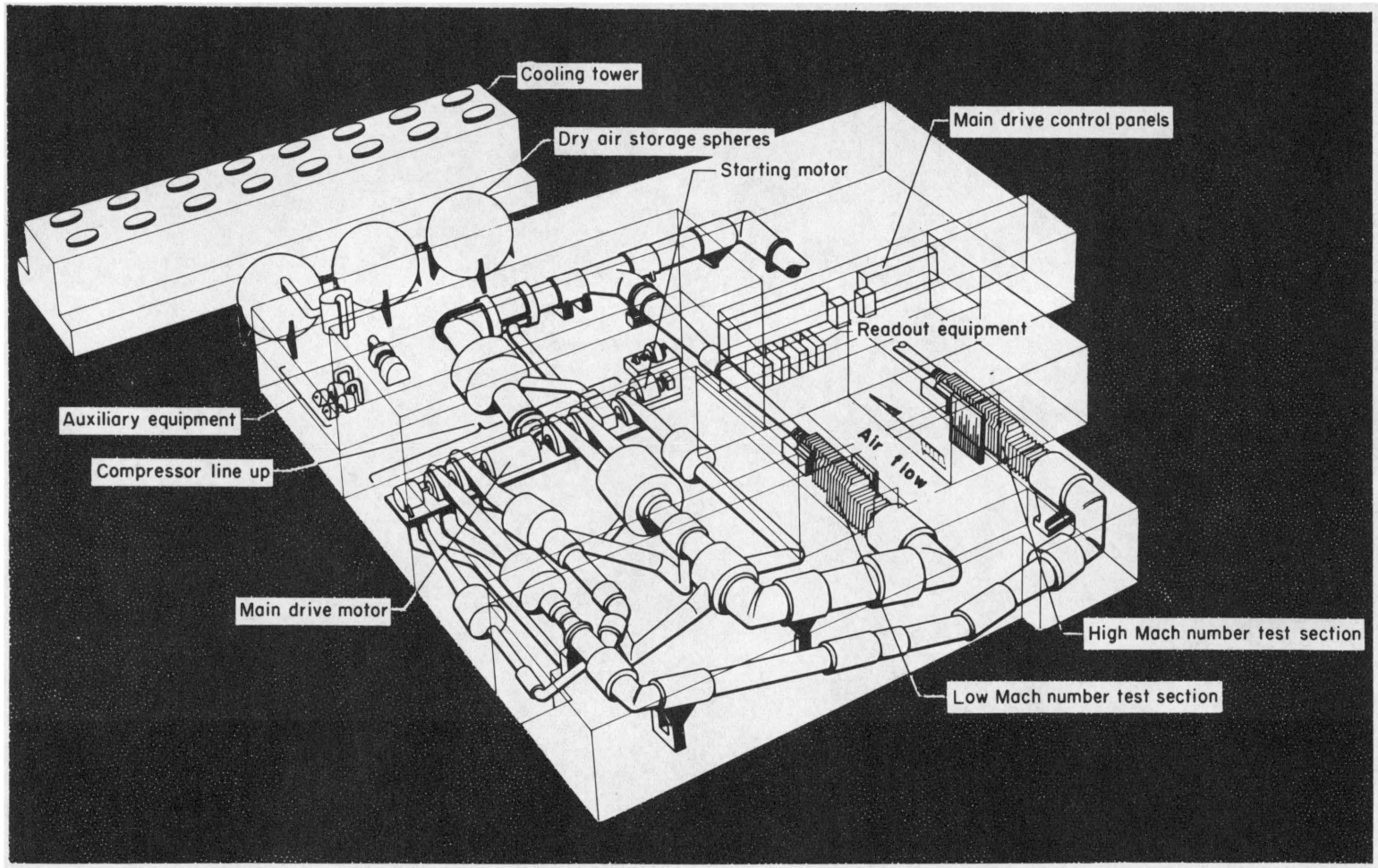

Figure 9.- Schematic layout of the test facility.

design and calibration is presented in reference 13. The variation is obtained by translating the lower block along a straight line parallel to the test section center line. A typical section of the nozzle is presented in Figure 8.

The stagnation pressure and temperature required for the tests may be controlled independently.

The model is mounted on a sting-balance combination. The sting is then mounted on an adjustable angle coupling in the tunnel (see Fig. 8). The outputs of the balance are then carried through wiring to the readout equipment as mentioned previously.

INSTRUMENTATION

The forces and moments on the model were obtained from an internally-mounted electrical strain-gage balance. It is important to mention that this balance was temperature compensated, that is, a suitable additional resistance was put in the gages to account for temperature effects upon their outputs. The design and fabrication of this type of balance is outlined in reference 14.

Since the results presented herein are for the condition of zero base pressure, the accurate measurement of pressures at the bases of the models is extremely important. This is a consequence of adjusting the gross measured drag data (see corrections and accuracies) to a condition of zero base drag. (In fact, it is vitally important for the models considered in this analysis, because the ratio of base area to wing area is larger than for most common airplane configurations.) In order to avoid

difficulties in measuring the pressures over the base, the base was machined back into the model leaving only a knife-edge base annulus and providing a chamber in which the pressures might be expected to be more uniform. Details of the bases of the two models are presented in Figures 10 and 11. Further, to obtain an adequate survey of the pressures in the cavity and along the lip from the base into the cavity, a 32-tube pressure rake was installed. Radial, angular and longitudinal locations of the individual tubes are presented in Figures 10 and 11. These pressure measurements were made on a manometer board utilizing alkazene as a working fluid.

TEST CONDITIONS

The conditions for the test are summarized in the following table:

	Model	
	Semiconical body with arrow wing	3/4-power semibody with diamond wing
Mach number	3.35	3.35
Reynolds number, based on M.A.C.	2.20×10^6	3.36×10^6
Dynamic pressure, psf	361	361
Stagnation pressure, psia . . .	19.6	19.6
Stagnation temperature, $^{\circ}F$ . .	150	150
Dewpoint, $^{\circ}F$	<-30	<-30
Angle-of-attack range, deg . .	-4 to 10	-4 to 10

Transition was fixed on both the models in order to insure a completely turbulent boundary layer. The details concerning the location

Table of Tube Locations

Tube No.	ø (deg)	R (in.)
1	0	0.50
2	0	2.00
3	90	0.50
4	90	0.50
5	112.5	0.63
6	135	0.75
7	157.5	1.25
8	157.5	1.88
9	168.5	2.00
10	168.5	2.08
11	180	0.50
12	180	1.25
13	180	2.00
14	180	2.50
15	180	2.90
16	180	3.05
17	180	3.20
18	202.5	2.00
19	202.5	2.38
20	202.5	2.95
21	225	1.25
22	225	2.00
23	225	2.70
24	247.5	1.25
25	247.5	2.00
26	247.5	2.60
27	270	0.50
28	270	1.25
29	270	2.00
30	270	2.25
31	270	2.35
32	270	2.45

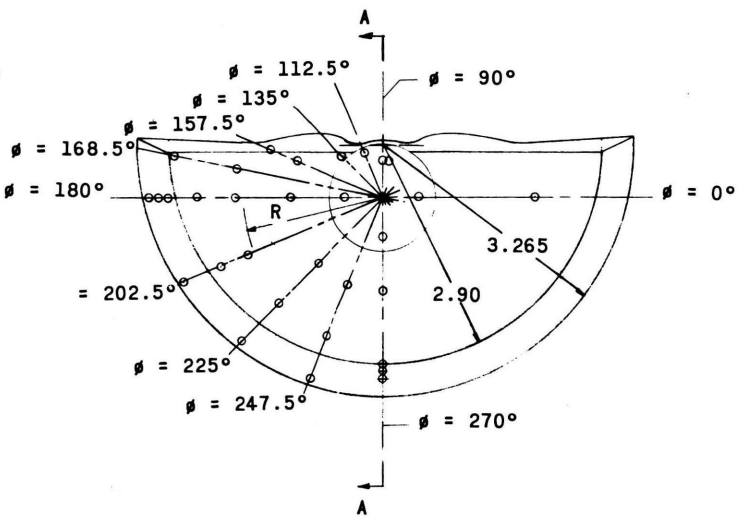

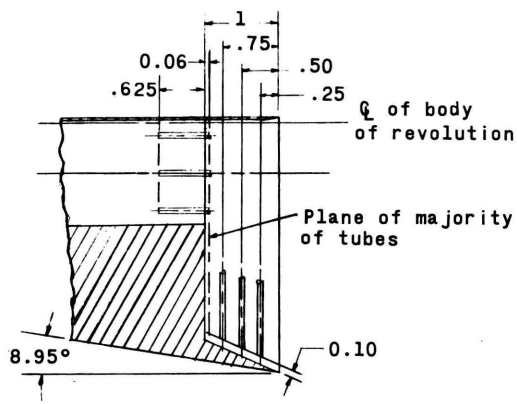

A-A

Figure 10.- Details of the base of the semiconical body. Dimensions are in inches unless otherwise noted.

Table of Tube Locations

Tube No.	ϕ (deg)	R (in.)
1	0	0.50
2	0	1.90
3	90	0.50
4	90	0.50
5	112.5	0.50
6	135	0.50
7	157.5	0.56
8	157.5	0.63
9	168.5	0.50
10	168.5	1.90
11	180	0.50
12	180	0.50
13	180	1.90
14	180	2.45
15	180	2.70
16	180	2.75
17	180	2.80
18	202.5	1.80
19	202.5	2.20
20	202.5	2.70
21	225	1.77
22	225	2.07
23	225	2.60
24	247.5	1.25
25	247.5	2.00
26	247.5	2.50
27	270	0.50
28	270	1.30
29	270	1.90
30	270	2.30
31	270	2.37
32	270	2.45

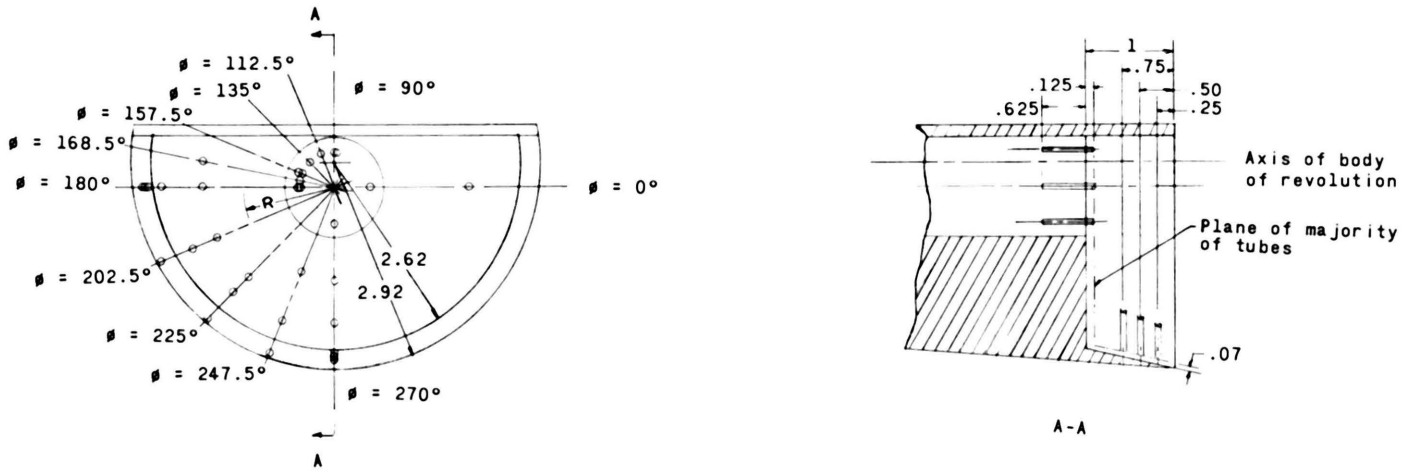

Figure 11.- Details of the base of the 3/4 power semibody. Dimensions are in inches unless otherwise noted.

CONFIDENTIAL

and width of the transition strips, and grit size were obtained from an unpublished prospective report of the Low Turbulence Branch of the NACA, Langley. The strips suggested were 1/16-inch wide located on the upper and lower surface at a constant 10 percent of the streamwise chord. The grit selected was No. 60 carborundum grains with a mean grit height of approximately 0.013 inch imbedded in Krylon. A similar strip was wrapped around the periphery of the body at the location of the lower wing surface strip intersection with the body.

CORRECTIONS AND ACCURACIES

The tunnel, as yet, has not been completely calibrated; however, preliminary indications are that the longitudinal pressure gradients are small, and thus the buoyancy effects on the model can be considered negligible. The Mach number in the test section is within ±0.015 of the value quoted.

Preliminary calibrations indicate flow misalignments exists in the angle of attack plane. To determine the value of the flow misalignment, tests were made with the model mounted upright and inverted. Plots of the normal force with angle of attack from the two runs were compared, and half the difference in the angle of attack for the two runs at an equal value of normal force gave the flow misalignment angle. This increment (an upflow in the tunnel) was added to the test geometric angles of attack. The angles of attack were corrected for deflection of the sting-balance combination under load in addition to the above correction.

The drag results presented in this paper were determined by adjusting the gross measured drag to condition of zero base drag, that is, the pressures on the base of the model were adjusted to a condition for free-stream static pressure on the base. Since the variation of pressure in the cavity at the base was extremely small, the pressure on the base of the model was selected to be the average of the measurements by the 32 tubes.

The accuracies of the various measured quantities based on a balance calibration and repeatibility of data are:

C_L	± 0.003
C_D'	± 0.0010
C_{D_b}	± 0.0005
α, deg	± 0.1

VI. PRESENTATION AND DISCUSSION OF RESULTS

The results are presented about the system of axes shown in Figure 12 and comparisons of the experimental and analytical results are presented in Figures 13 through 18.

Typical schlieren photographs taken at angles of attack of approximately -4°, 0°, 4°, and 10° are presented for the arrow wing configuration and the diamond wing configuration in Figures 13(a) and 13(b), respectively.

The experimental variations of base drag coefficient with angle of attack are shown in Figure 14 for the two models. These are the drag values which were subtracted from the gross measured drag to obtain the drag coefficients presented.

The remainder of the figures show comparisons between the theoretical and experimental results. Figures 15(a) and 15(b) give a comparison of the theoretical and experimental variation of lift coefficient with angle of attack for the arrow wing configuration, and the diamond wing configuration, respectively. In Figures 16(a) and 16(b), the theoretical and experimental variation of drag coefficient with angle of attack is given for the arrow wing configuration and the diamond wing configuration, respectively. Plots of the theoretical and experimental variation of the drag coefficient with lift coefficient squared are given in Figures 17(a) and 17(b). Figures 18(a) and 18(b) summarize the above comparisons by showing the theoretical and experimental variation of drag coefficient and lift-drag ratio with lift coefficient for each of the models.

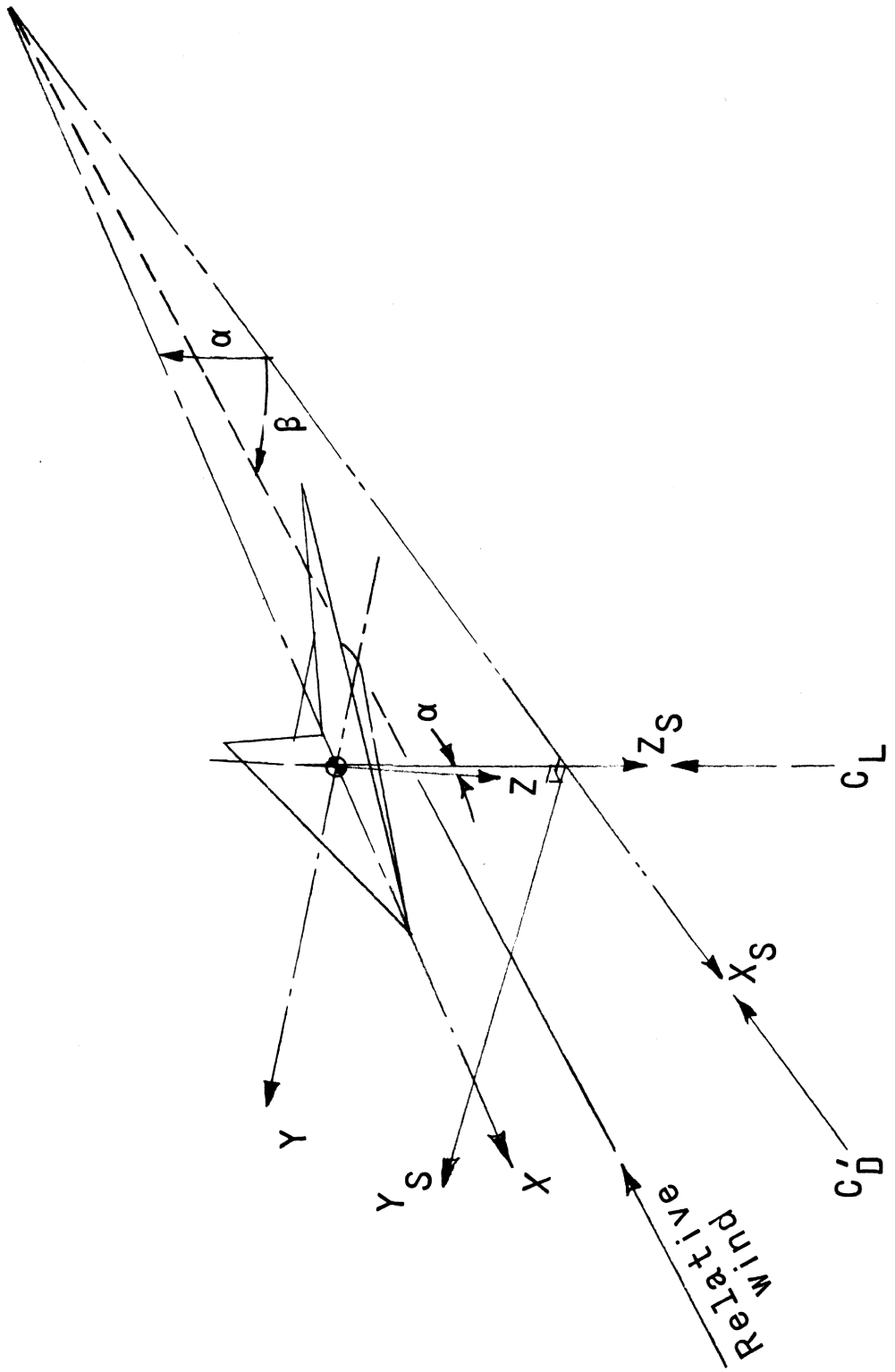

Figure 12.- System of axes.

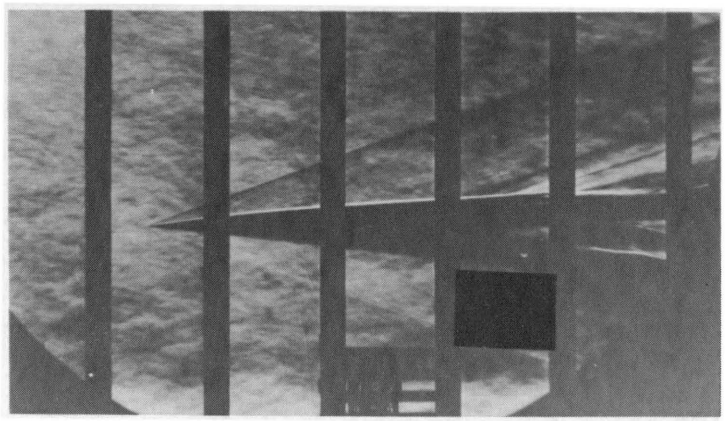

α = -4.0°

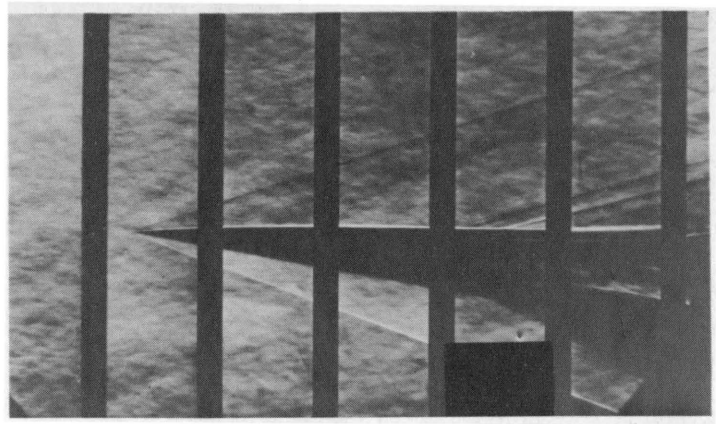

α = 0.2°

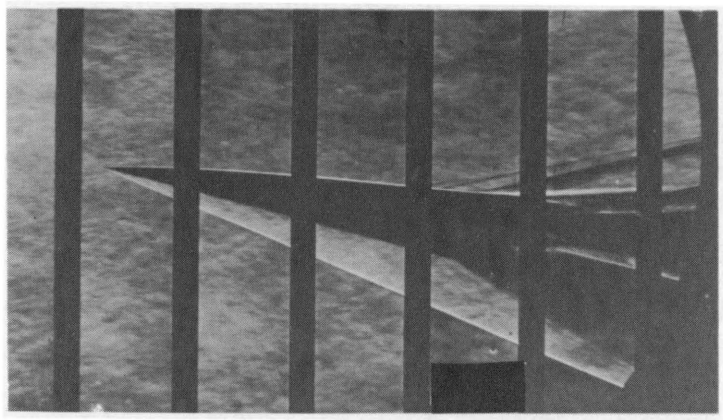

α = 4.4°

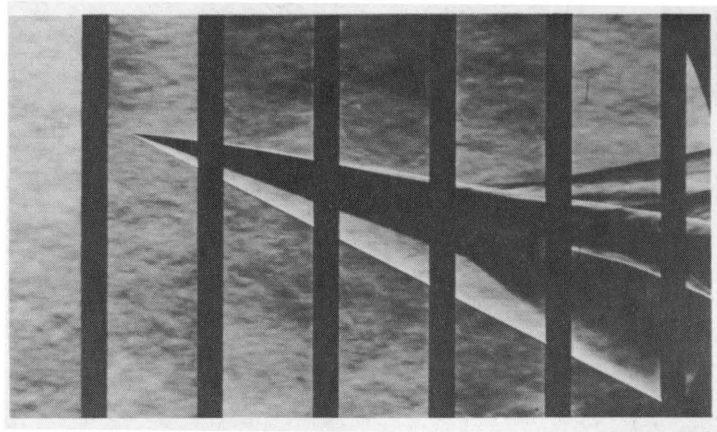

α = 10.8°

(a) Arrow wing configuration. L-58-1624

Figure 13.- Typical schlieren photographs of the models. M = 3.35; fixed transition.

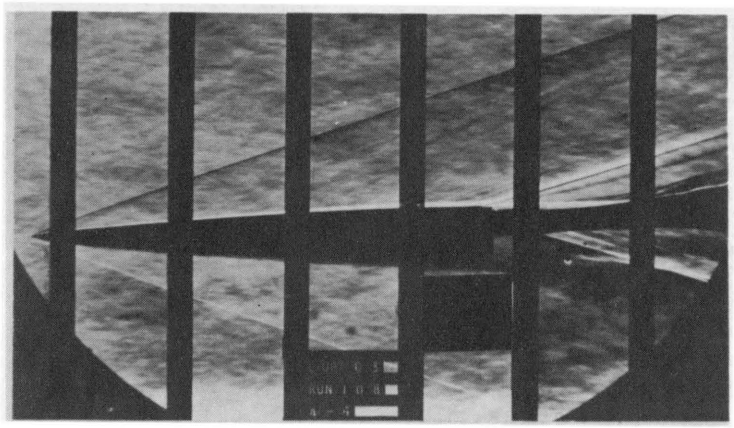

α = -4.2°

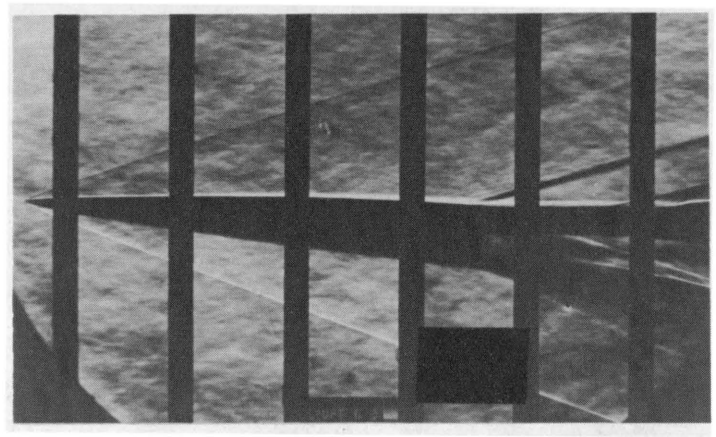

α = 0.2°

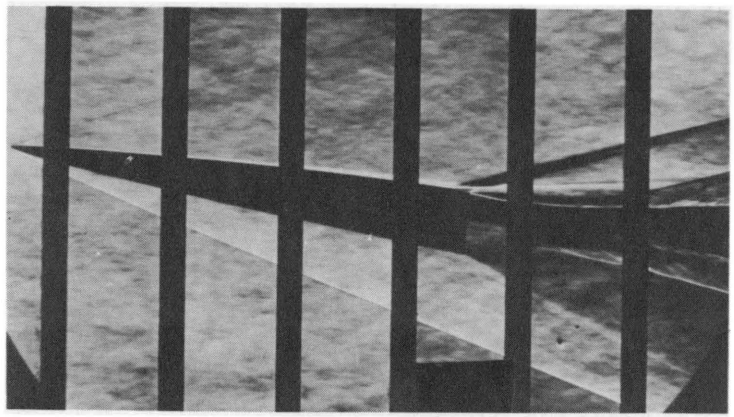

α = 4.7°

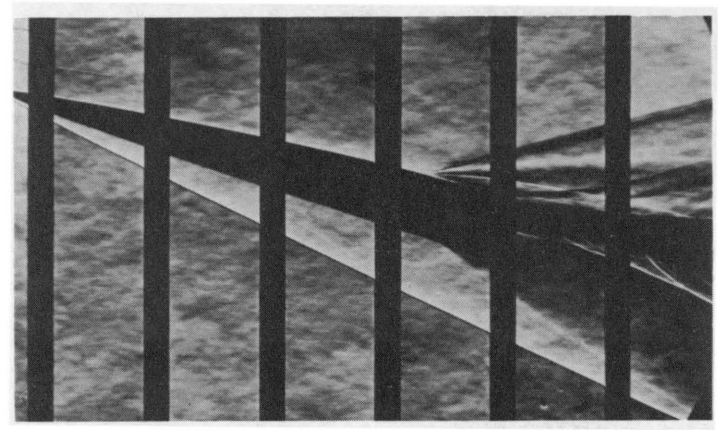

α = 11.3°

(b) Diamond wing configuration. L-58-1625

Figure 13.- Concluded.

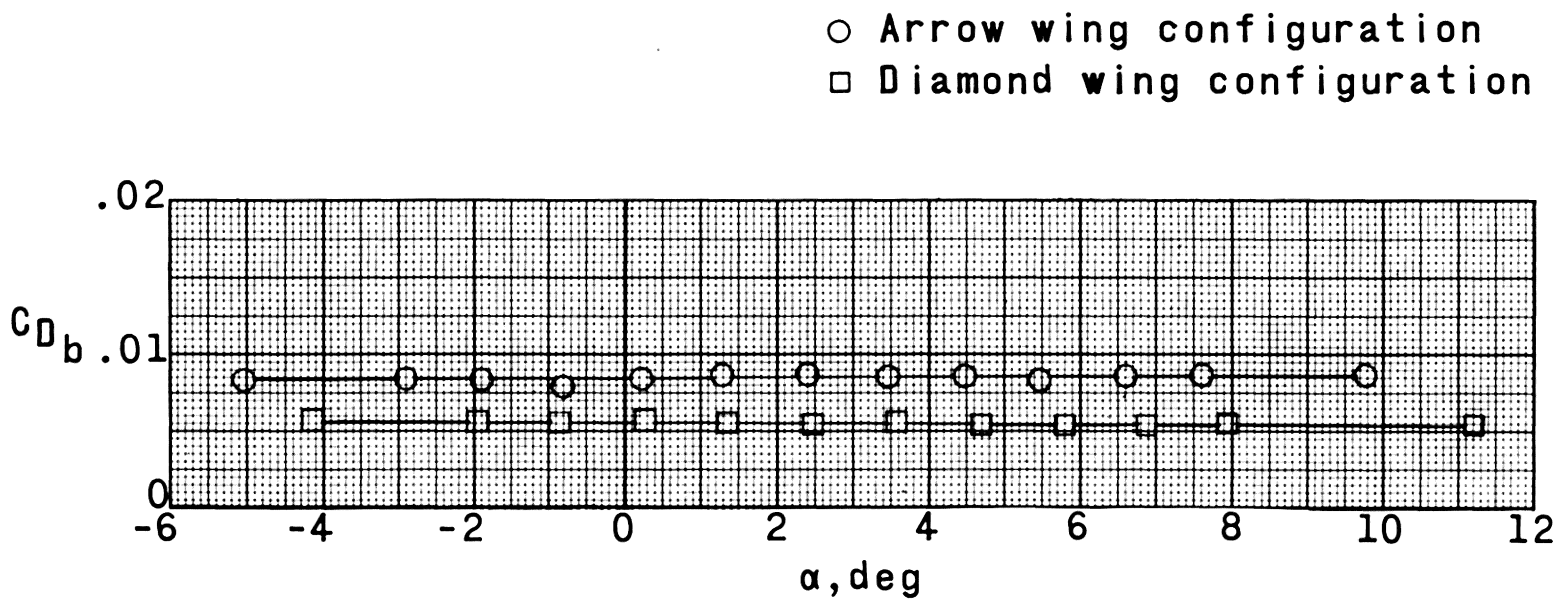

Figure 14.- Variation of the experimental base drag coefficient with angle of attack. M = 3.35.

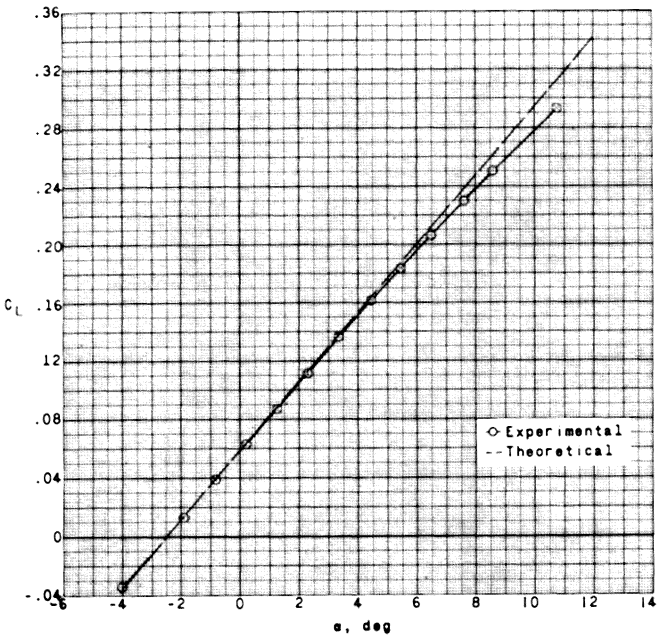

(a) Arrow wing configuration.

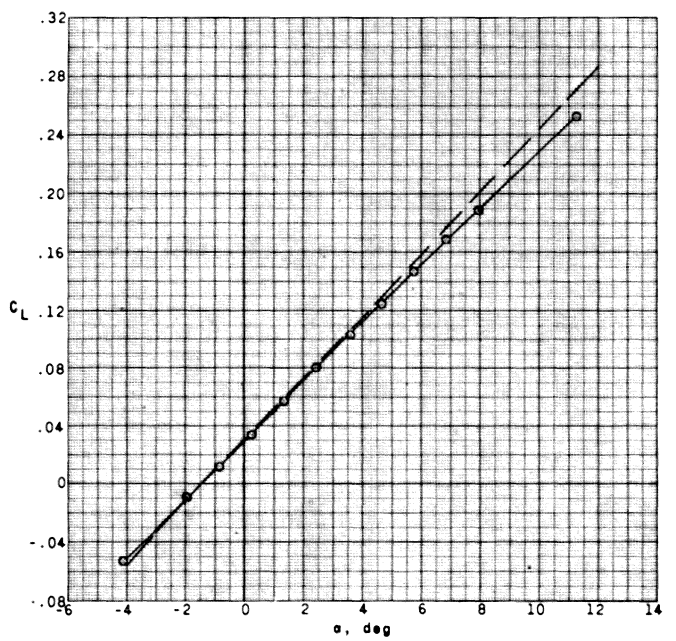

(b) Diamond wing configuration.

Figure 15.- Comparison of the theoretical and experimental variation of lift coefficient with angle of attack. M = 3.35.

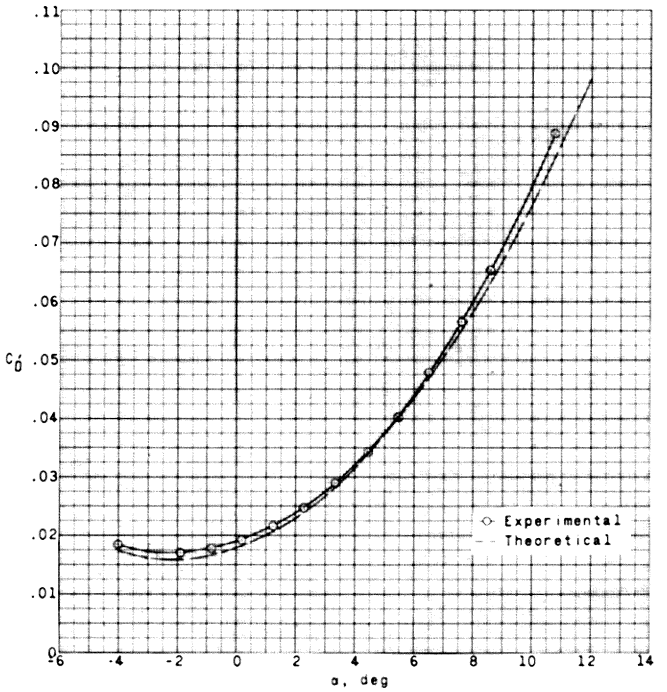

(a) Arrow wing configuration.

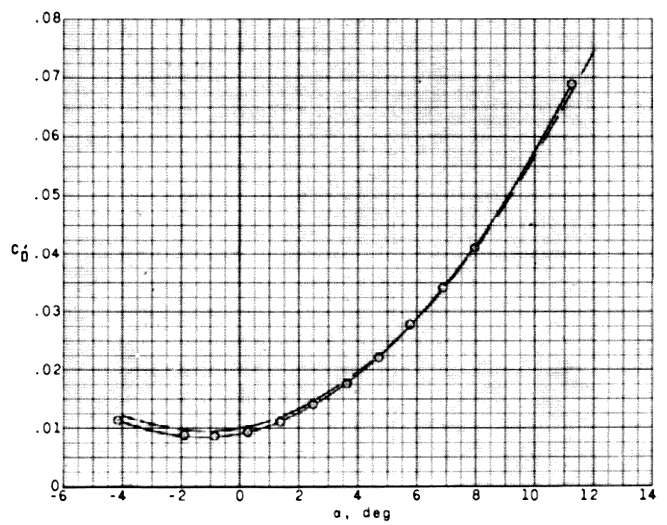

(b) Diamond wing configuration.

Figure 16.- Comparison of the theoretical and experimental variation of drag coefficient with angle of attack. M = 3.35.

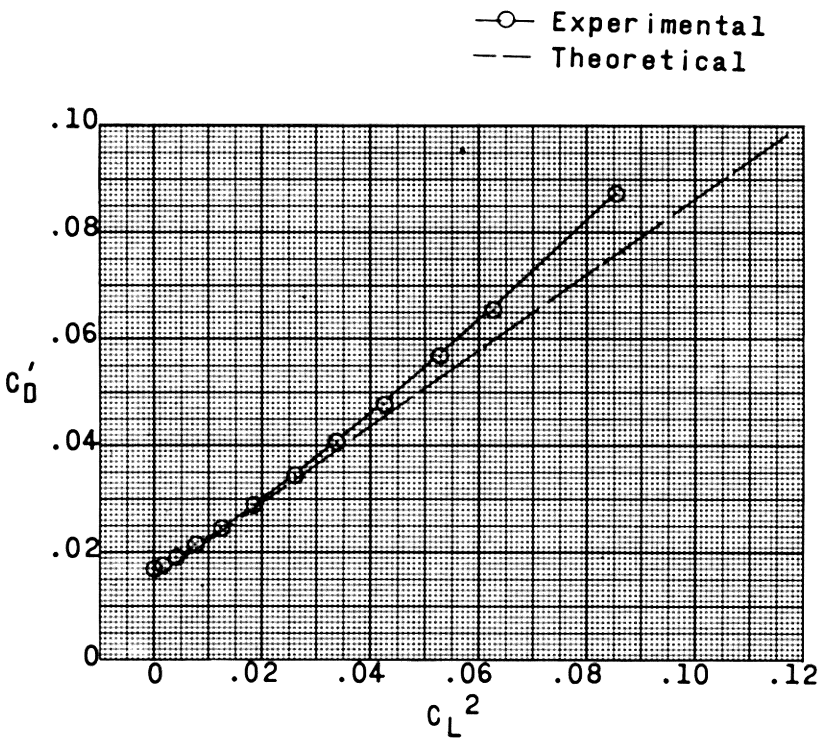

(a) Arrow wing configuration.

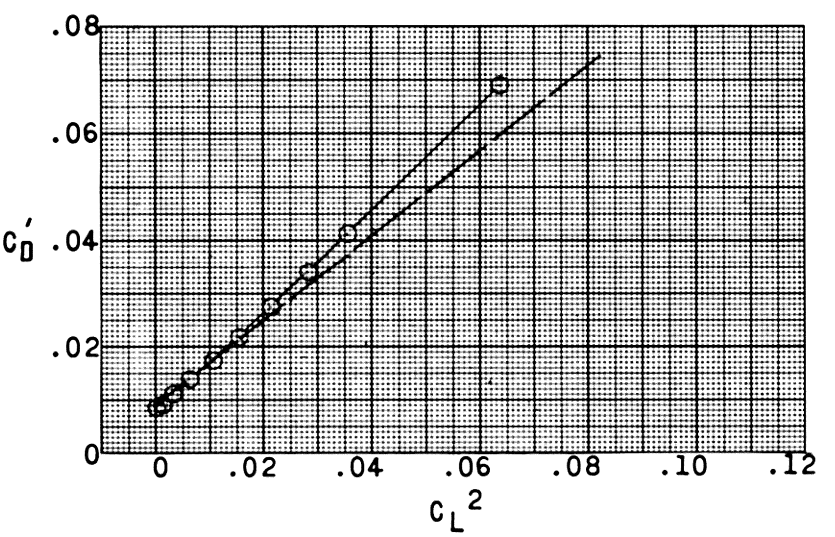

(b) Diamond wing configuration.

Figure 17.- Comparison of theoretical and experimental variation of drag coefficient with lift coefficient squared. M = 3.35.

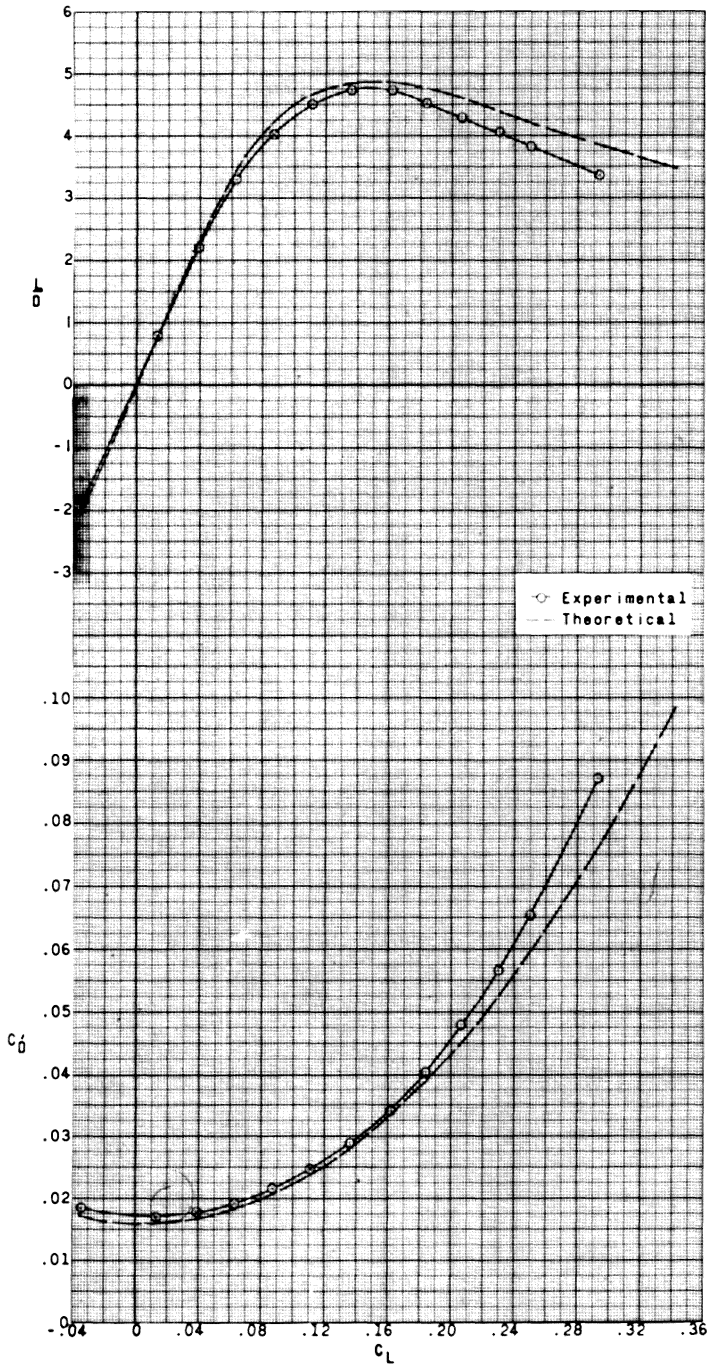

(a) Arrow wing configuration.

Figure 18.- Comparison of the theoretical and experimental variation of drag coefficient and lift-drag ratio with lift coefficient. M = 3.35.

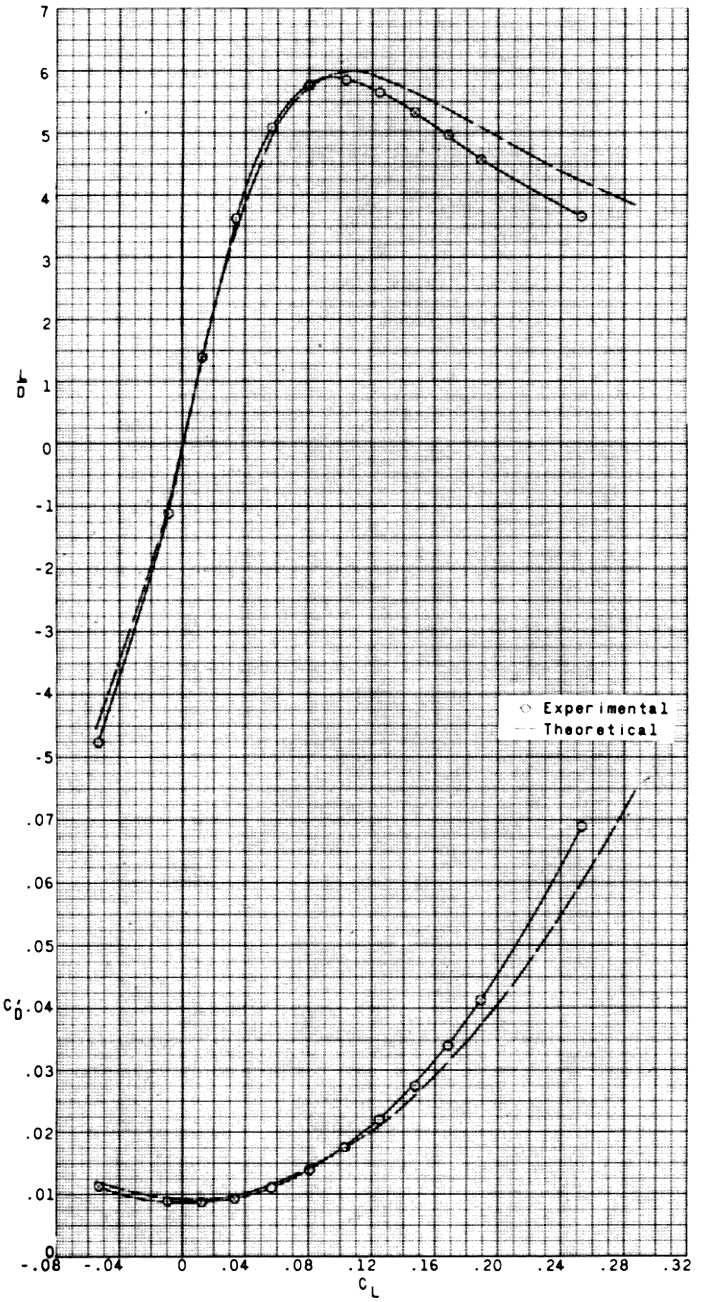

(b) Diamond wing configuration.

Figure 18.- Concluded.

A discussion of the above results is now in order.

The schlieren photographs shown in Figures 13(a) and 13(b) provide an accurate description of the shock and expansion patterns created by the models at a Mach number of 3.35. A rough check of the coordinates and sweep of the bow shock at zero angle of attack, seem to indicate excellent agreement with the theoretical values. This is to be expected and gives confidence in the analytical results, since the zero angle of attack case was dependent on an accurate evaluation of the flow field by the method of characteristics.

The values of the experimental base drag coefficients given for each of the models in Figure 14 show clearly the necessity of measuring base drag with great care. A comparison of these results with the drag results presented in the later figures shows the base drag coefficients at zero angle of attack are approximately 30 and 40 percent of the gross measured drag for the arrow wing configuration and the diamond wing configuration, respectively. The significance of the zero angle of attack drag coefficient will be brought out later in the discussion, but it is sufficient to say here that the accuracy of its measurement is important. The author feels his instrumentation was sufficiently adequate to insure that the accuracy of the values shown in Figure 14 is within the limits given on page 47.

Before presenting the comparisons of the theoretical and experimental lift and drag coefficients, it is first important to develop the expression for the maximum lift-drag ratio. This will permit the assessment of the relative importance of the various terms in the lift and drag

relations in affecting the accuracy of predicting the maximum lift-drag ratio analytically. To accomplish this we divide equation (10) by equation (11) and we have

$$\frac{L}{D} = \frac{C_{L_o} + C_{L_\alpha}\alpha}{C_{D_o} + \left(C_{L_o} + G\right)\alpha + C_{L_\alpha}\alpha^2} \tag{13}$$

Upon differentiating equation (13) with respect to α and setting the derivative equal to zero, we get the maximum lift-drag ratio expression

$$\left(\frac{L}{D}\right)_{max} = \frac{C_{L_\alpha}}{2\sqrt{-C_{L_o}G + C_{L_\alpha}C_{D_o}} - C_{L_o} + G} \tag{14}$$

Keeping this expression in mind, we will examine the correlation between the theoretical and experimental results, and note the possible effects of errors in the analysis on the maximum lift-drag ratio.

The accuracies of the lift at zero angle of attack C_{L_o} and the lift-curve slope C_{L_α} will be discussed first. In Figures 15(a) and 15(b) we find the lift at zero angle of attack which was evaluated with the use of the method of characteristics to be given almost exactly for both configurations. A comparison of the theoretical and experimental lift-curve slopes at small angles of attack also shows good agreement for both configurations. In fact, the arrow wing configuration shows perfect agreement, while for the diamond configuration an experimental C_{L_α} value of 0.0195 per degree was obtained as compared to a slightly higher theoretical value of 0.021 per degree. At higher angles of attack the analysis gave higher values of lift coefficient than were measured experimentally

for both configurations. This decrease in the experimental lift at high angles of attack is associated with viscous flow separation on the inboard sections of the upper surface of the wing. However, this result is to be expected; since for the analysis the flow was assumed to be inviscid. Further, we can expect the analysis to overestimate the maximum lift-drag ratio.

The drag coefficients as given by the analysis are treated next by examining their variation with angle of attack in Figure 16(a) and 16(b). The value of drag at zero angle of attack, C_{Do}, is found to be underestimated for the arrow wing configuration, while it is overestimated for the diamond wing configuration (Fig. 16(b)). These errors possibly are a combination of the individual errors in estimating the items which combine to give C_{Do}; however, since the same analysis was used for both models, it would not seem legitimate to adjust any of the individual items. Further, the absence of the interference drag in the analysis could possibly explain the differences between the results of the analysis and the experiment. Upon further examination of the curves, we see that the drag at angles of attack greater than zero is underestimated by the analysis. This is a consequence of the aforementioned effect on the analytical results of not considering the viscous separation. The failure of a wing-body combination at angle of attack to achieve the theoretically predicted lift due to viscous separation is also associated with higher values of drag at these lift coefficients. To more clearly illustrate this point a plot of the drag coefficient versus the square of the lift

coefficient is presented in Figure 17(a) and 17(b) for the arrow wing configuration and the diamond wing configuration, respectively. The slopes of these curves, $\frac{\Delta C_D}{C_L^2}$, are known as the drag-due-to-lift factors, and for the case of no leading-edge suction on the wing the theoretical value of drag-due-to-lift is given by $\frac{1}{C_{L_\alpha}}$. By measuring the slopes of the experimental curves we find the drag-due-to-lift factors to be 0.8 for the arrow wing configuration and 0.9 for the diamond wing configuration as compared to $\frac{1}{C_{L_\alpha}}$ values of 0.74 and 0.82, respectively. These higher experimental drag-due-to-lift factors clearly illustrate the effect of viscous separation on the comparison of the theoretical and experimental results.

Although the lift and drag terms are treated separately in equation (14), the above discussion will help to explain the differences in the comparison of the theoretical and experimental variation of drag coefficient and lift-drag ratio with lift coefficient presented in Figures 18(a) and 18(b) for the two configurations. At low lift coefficients, where fairly good correlation is found between the analysis and experiment, the errors in lift-drag ratio are small while at higher values the errors become magnified. Fortunately, the lift coefficient for maximum lift-drag ratio is in the low lift range and only small errors result. The maximum lift-drag ratios for the arrow wing configuration (Fig. 18(a)) were 4.85 from the analysis as to compared to 4.77 from the experiment, while those for the diamond wing configuration

(Fig. 18(b)) were 6.0 from the analysis as compared to 5.9 from the experiment. Although exact correlations between the analysis and the experiment were not obtained for the individual lift and drag terms of the maximum lift-drag ratio equation, equation (14), it can be said that the final results of the analysis give excellent agreement with experiment.

VII. CONCLUSIONS

An analytical method for predicting the lift-drag relations of flat-top wing-body combinations has been developed. The analysis was based on the following assumptions: (1) the linear theory was applicable, (2) the leading edge of the wing was coincident with the bow shock produced by the body, and (3) the base drag was zero, that is, the static pressure at the base was equal to free stream static pressure. The individual terms, which when combined together give the total expressions for the lift and drag coefficients, were evaluated by recent theoretical methods. The results of this analysis were compared to experimental data for two flat-top wing-body combinations at a Mach number of 3.35. These combinations were a semiconical body mounted beneath an arrow wing, and a 3/4-power semibody mounted beneath a diamond wing with the wing and body apexes being coincident. From a comparison of the theoretical and experimental results of this investigation, the following conclusions are made:

1. The accuracy of determining the lift coefficient at zero angle of attack by use of the method of characteristics is excellent for both configurations. The lift-curve slopes (taken at small α's) also showed excellent agreement between the theoretical and experimental results for both configurations. At higher angles of attack, however, the theoretical values of lift were higher than the experimental values for both configurations. This decrease in experimental lift was associated with viscous flow separation on the inboard sections of the upper surface of the wing. However, this result was to be expected; since for the analysis

the flow was assumed to be inviscid. In addition it was further illustrated that viscous flow separation gave higher drag-due-to-lift factors experimentally than were predicted theoretically by the relation $\frac{\Delta C_D}{C_L^2} = \frac{1}{C_{L_\alpha}}$ for the case of no leading-edge suction.

2. The value of drag coefficient at zero angle of attack for the arrow wing configuration was underestimated, while that for the diamond wing configuration was overestimated. These differences could be attributed to errors in evaluating the individual terms, such as, the body pressure drag, the wing wave drag, or the skin friction drag. In addition, a further cause could be the lack of interference drag in the analysis.

3. Although errors were found in exactly predicting the lift-drag characteristics of the two configurations, the accuracy of the important result, maximum lift-drag ratio, was found to be good as given by the analysis. The values of maximum lift-drag ratio for the arrow wing configuration were 4.85 as given by the analysis compared to 4.77 from the experiment, while the diamond wing configuration values were 6.0 and 5.9, respectively.

These results indicate that the analysis is reasonably accurate for predicting the lift and drag characteristics of flat-top wing-body combinations. Further work which would include the interference drag at zero angle of attack should be done in order to obtain better correlations between theory and experiment. Since the viscous effects are nonlinear, they do not lend to a rigorous analytical treatment; however, the

derivation of an empirical formula for lift-curve slope, which would include this item, would be of great value in obtaining even more accurate analytical results.

VIII. SUMMARY

An analytical method for predicting the lift and drag characteristics of flat-top wing-body combinations has been developed. The analysis was applied to two configurations. These were a semiconical body mounted beneath an arrow wing and a 3/4-power semibody mounted beneath a diamond wing with the wing and body apexes being coincident.

Wind tunnel tests were performed at a Mach number of 3.35 on the two models to obtain an experimental verification of the results as predicted by the analysis. The comparisons of the theoretical and experimental results showed slight inaccuracies in the individual terms which contribute to the lift and drag expressions. These inaccuracies were primarily attributed to the lack of some considerations (e.g., wing-body drag interference at zero angle of attack, and viscous separation at angles of attack greater than zero) in the analysis.

The end result (namely, the maximum lift-drag ratio), however, was predicted with reasonable accuracy by the analysis. The values of maximum lift-drag ratio for the arrow wing configuration were 4.85 from the analysis as compared to 4.77 from experiment, while the results for the diamond wing configuration were 6.0 and 5.9, respectively.

IX. ACKNOWLEDGMENTS

The author wishes to express his appreciation to the National Advisory Committee for Aeronautics for the permission to use material in this thesis which was obtained from a research project conducted at the Langley Laboratory.

In particular, the author wishes to express his gratitude to the staff of the Langley Unitary Plan wind tunnel who assisted in the calculation of the data and the preparation of this thesis.

He also wishes to thank Dr. R. W. Truitt of the Aeronautical Engineering Department of the Virginia Polytechnic Institute for his advise and assistance in preparing this thesis.

X. BIBLIOGRAPHY

1. Ferri, Antonio, Clarke, Joseph H., and Casaccio, Anthony: Drag Reduction in Lifting Systems by Advantageous Use of Interference. PIBAL Rep. 272, Dept. Aero. Eng. Appl. Mech., Polytechnic Inst. Brooklyn, May, 1955.

2. Eggers, A. J., Jr., and Syvertson, Clarence A.: Aircraft Configurations Developing High Lift-Drag Ratios at High Supersonic Speeds. NACA RM A55L05, 1956.

3. Syvertson, Clarence A., Wong, Thomas, J., and Gloria, Hermilo R.: Additional Experiments With Flat-Top Wing-Body Combinations at High Supersonic Speeds. NACA RM A56I11, 1957.

4. Jorgensen, Leland H.: Elliptic Cones Alone and With Wings at Supersonic Speeds. NACA TN 4045, 1957.

5. Jorgensen, Leland H.: Experimental Lift-Drag Ratios For Two Families of Wing-Body Combinations at Supersonic Speeds. NACA RM A58A08, 1958.

6. Reyn, John W., and Clarke, Joseph H.: An Assestment of Body Lift Contributions and of Linearized Theory for Some Particular Wing-Body Configurations. PIBAL Rep. 305, Dept. of Aero. Eng. and Appl. Mech., Polytechnic Inst. of Brooklyn, June, 1956.

7. Migotsky, Eugene, and Adams, Gaynor J.: Some Properties of Wing and Half-Body Arrangements at Supersonic Speeds. NACA RM A57E15, 1957.

8. Kopal, Zdenek: Tables of Supersonic Flow Around Cones. Tech. Rep. No. 1, M.I.T., Dept. of Elec. Eng., Center of Analysis, Cambridge, Mass., 1947.

9. Beane, Beverly: The Characteristics of Supersonic Wings Having Biconvex Sections. Jour. Aero. Sci., vol. 18, no. 1, Jan. 1951, pp. 7-20.

10. Grant, Frederick C., and Cooper, Morton: Tables For the Computation of Wave Drag of Arrow Wings of Arbitrary Airfoil Section, NACA TN 3185, 1954.

11. Rubesin, Morris, W. Maydew, Randall C., and Varga, Steven A.: An Analytical and Experimental Investigation of the Skin Friction of the Turbulent Boundary Layer on a Flat Plate at Supersonic Speeds. NACA TN 2305, 1951.

12. Harmon, Sidney, M., and Jefferys, Isabella: Theoretical Lift and Damping in Roll of Thin Wings With Arbitrary Sweep and Taper at Supersonic Speeds. NACA TN 2115, 1950.

13. Burbank, Paige B., and Byrne, Robert W.: The Aerodynamic Design and Calibration of an Asymmetric Variable Mach Number Nozzle With a Sliding Block For the Mach Number Range 1.27 to 2.75. NACA TN 2921, 1953.

14. Hansen, Raymond M.: Mechanical Design and Fabrication of Strain-Gage Balances. Presented to Wind Tunnel and Model Testing Panel of AGARD (Rome, Italy), Feb. 20-25, 1956.

15. Shapiro, Ascher H.: The Dynamics and Thermodynamics of Compressible Fluid Flow. Vol. II, The Ronald Press Co., 1954, pp. 676-682.

16. Ferri, Antonio: Elements of Aerodynamics of Supersonic Flows. The Macmillan Co., 1949, pp. 361-362.

The vita has been removed from the scanned document

XII. APPENDICES

APPENDIX A

A BRIEF OUTLINE OF THE METHOD OF CHARACTERISTICS AND ITS APPLICATION TO THE SOLUTION OF THE FLOW AROUND A BODY OF REVOLUTION

For a body of revolution, whose axis is parallel to the undisturbed flow, we have the case of an axial-symmetric flow. As a result of this type of flow, the physical phenomenon are the same in every meridian plane. Therefore, we need only to consider the variation of the flow properties in one plane; because no variations occur in a direction normal to any meridan plane. The equation of potential flow is then dependent on only two variables. A choice of the cylindrical coordinates is chosen and the equation is (see ref. 15)

$$\left(1 - \frac{u^2}{a^2}\right)\phi_{xx} - \frac{2uv}{a^2}\phi_{xr} + \left(1 - \frac{v^2}{a^2}\right)\phi_{rr} + \frac{\phi_r}{r} = 0 \qquad \text{(A1)}$$

where

$$a^2 = a_0^2 - \frac{(\bar{\gamma} - 1)V^2}{2} = a_0^2 - \frac{(\bar{\gamma} - 1)}{2}\left(u^2 + v^2\right)$$

and

$$u = \frac{\partial\phi}{\partial x} = \phi_x \qquad v = \frac{\partial\phi}{\partial r} = \phi_r$$

Equation (A1) could be written as

$$A\phi_{xx} + 2B\phi_{xr} + C\phi_{rr} = D \qquad (A2)$$

where

$$A = a^2 - u^2 \qquad B = -uv \qquad C = a^2 - v^2 \qquad D = \frac{-a^2 v}{r}$$

Solutions of equation (A2) with real roots are obtained, when the equation is of the hyperbolic type ($B^2 - AC > 0$). These solutions are known as the characteristic curves. The characteristic curves in the physical and hodograph planes are described by, respectively,

$$\left(\frac{dr}{dx}\right)_{I,II} = \tan(\theta \mp \alpha) \qquad (A3)$$

$$\frac{1}{V}\left(\frac{dV}{d\theta}\right)_{I,II} = \mp\tan\alpha + \frac{\sin\alpha \tan\alpha \sin\theta}{\sin(\theta \mp \alpha)} \frac{1}{r}\left(\frac{dr}{d\theta}\right)_{I,II} \qquad (A4)$$

The relation between the characteristics and the streamlines is shown in the sketch. In order to determine the physical characteristics of the flow, equations (A3) and (A4) must be solved simultaneously, that is, both the physical and hodograph characteristics must be constructed simultaneously. The construction of the two families of characteristic curves is accomplished by replacing the system of continuous characteristic curves by a series of straight line chords which connect the intersection points of the two curves of the two families. The solution for the coordinates of these intersections and the physical properties at these points is obtained by

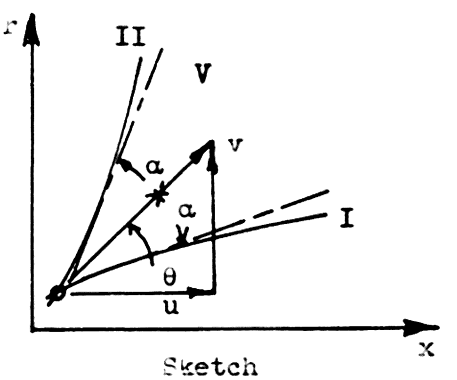

Sketch

writing equations (A3) and (A4) in a finite difference equation. An iteration procedure utilizing the results from the first application of the finite difference equation is used to obtain more accurate results.

An example using the above method to determine the characteristics net about a body of revolution is given in reference 15. The most important step in the example is to assume that the body for a small percentage of the body length is conical, and thus the calculation can be started by determining the conical flow field at the nose. The peculiarity of the conical field is that the physical properties (for example, the pressure) are constant along a ray originating from the body apex. The properties of this field can then easily be determined with the use of the Kopal tables (ref. 8). From the cone calculations the characteristics lines from the base of the finite body of revolution to the nearest ray and then from ray to ray out to the shock can be determined from the characteristic equations. From the intersection of these characteristic lines and the rays from the body apex, the net is constructed out to any desired point in the flow field surrounding the body. For bodies of finite length, such as the ones considered in the analysis, the net beyond the body is constructed by assuming that beyond the base of the body there is an infinite cylinder.

In the determination of the net the physical properties of the flow field are also determined. These include the coordinates, the local flow angle, and the total velocity vector at the intersection of the characteristic lines. The application of this information for determining

the body pressure drag and lift, and the body induced lift on surfaces placed in the field was described in the Analysis.

APPENDIX B

OUTLINE FOR DETERMINING THE LIFT-CURVE SLOPE EQUATION FOR WINGS WITH SUPERSONIC LEADING AND TRAILING EDGES

Since the evaluation of the lift curve slope involves integrating the disturbance pressure field over the wing at angle of attack, it is first important to define the linear (small disturbance) pressure relation. The incremental pressure coefficient is as follows:

$$\Delta C_p = \frac{4}{V_\infty} \phi_x \tag{B1}$$

where

V velocity in the free stream

ϕ disturbance velocity potential on the upper surface of the wing $\left(\phi_x = \frac{\partial \phi}{\partial x}\right)$

Now, the lift-curve slope is found by integrating this pressure distribution over the surface of the wing, and is, then

$$C_{L_\alpha} = \frac{1}{S\alpha} \iint_S \phi_x \, dx \, dy \tag{B2}$$

Then substituting equation (B1) into equation (B2), we have

$$C_{L_\alpha} = \frac{4}{VS\alpha} \iint_S \phi_x \, dx \, dy \tag{B3}$$

Thus, the only problem is to determine ϕ_x for our particular case of supersonic leading and trailing edges, and then perform the integration.

The expression for ϕ_x was determined in reference 12 by a proper choice of source and sink distributions which correspond to the planform geometry of our wings. In addition, the authors performed the integration of equation (B3), and obtained the following expression for the lift-curve slope.

$$C_{L_\alpha} = \frac{1}{\beta\pi\sqrt{m'^2 - 1}} \left\{ \frac{\left[4m's' + A'(s' - 1)\right]^2}{2A'\left(s'^2 - 1\right)} \left[\frac{1}{s'} \cos^{-1} \frac{1}{m'} + \frac{s'\sqrt{m'^2 - 1}}{\sqrt{(s'm' - 1)(s'm' + 1)}} \cos^{-1} - \frac{1}{s'm'} \right] - \pi \frac{\left[4s'm' - A'(s' - 1)\right]^2}{4A'(s' - 1)} \sqrt{\frac{m' + 1}{s'(s'm' + 1)}} \right\} \qquad (B4)$$

with the following restrictions:

$$\beta \cos \gamma > 1$$

$$A' > \frac{4\lambda m'}{(1 + \lambda)(m' - 1)}$$

Care must be taken in the formula to preserve the correct sign of the terms involving radicals. For example, if $a < 0$ and $b < 0$, then

$$\sqrt{ab} = \sqrt{(-1)^2 |a||b|} = -\sqrt{|a||b|}$$

The computations as suggested by the authors were carried out to seven significant figures to assure reliable results.

APPENDIX C

FORMULATION OF THE G EXPRESSION IN THE DRAG EQUATION

The effect of the angle of attack pressure field of the wing acting on the surface of the body is to be determined. The assumptions made are:

(a) The angle of attack pressure acting on the body is constant over the body and equal to the pressure at the root chord of the wing defined by $y = 0$ (see sketch)

(b) The leading edge of the wing is coincident with the body shock defined by $\cot \gamma = \tan X$

(c) The pressure coefficient is given by the linear relation

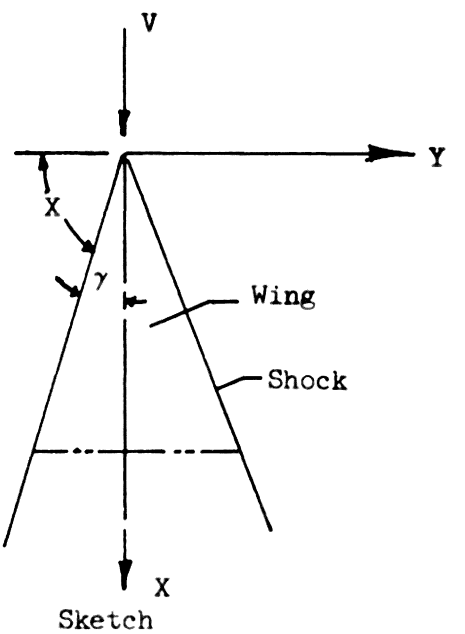

Sketch

$$C_p = -\frac{2\phi_x}{V_\infty} \tag{C1}$$

where ϕ is the disturbance-velocity potential.

An expression for a disturbance-velocity potential which satisfies the governing linearized compressible flow equation for the case considered here is given in reference 16. Since we are interested in the line $y = 0$, the expression for ϕ_x inside the Mach cone is required and is

$$\phi_x = \frac{-V\alpha}{\beta\sqrt{1 - n'^2}}\left(1 - \frac{2}{\pi}\sin^{-1}\sqrt{\frac{n'^2 - \sigma^2}{1 - \sigma^2}}\right) \tag{C2}$$

where

$$\sigma = \frac{y \tan X}{x}$$

$$n' = \frac{\tan X}{\beta}$$

$$\beta = \sqrt{M_\infty^2 - 1}$$

Thus, to get the pressure coefficient along $y = 0$, we substitute equation (C2) into equation (C1) and then

$$C_p\Big|_{y=0} = \frac{2\alpha}{\beta\sqrt{1 - n'^2}}\left(1 - \frac{2}{\pi}\sin^{-1}n'\right) \tag{C3}$$

Remembering that $\tan X = \cot \gamma = \frac{1}{\tan \gamma}$ we may rewrite (C3) after some manipulation as

$$C_p\Big|_{y=0} = \frac{2\alpha \tan \gamma}{\sqrt{\beta^2\tan^2\gamma - 1}}\left(1 - \frac{2}{\pi}\sin^{-1}\frac{1}{\beta \tan \gamma}\right) \tag{C4}$$

Now to get the drag coefficient associated with the body in the wing pressure field at angle of attack we write

$$\left(C_{D,B}\right)_W = \frac{\iint_{A_b} C_p \, dx \, dy}{S} \tag{C5}$$

because the pressure forces are projected onto the base. The evaluation of the integral becomes simplified since C_p is constant, and the $\iint_{A_b} dx\, dy$ = area of the base, or $\frac{\pi r_b^2}{2}$ for a body of revolution.

Therefore, substituting equation (C4), and the expression for the area of the base into equation (C5), we get the resultant drag coefficient expression,

$$\left(C_{D,B}\right)_W = \frac{r_b^2 \tan\gamma}{S\sqrt{\beta^2\tan^2\gamma - 1}}\,\alpha\left(\pi - 2\sin^{-1}\frac{1}{\beta\tan\gamma}\right) \tag{C6}$$

Now multiplying and dividing equation (C6) by 2, yields

$$\left(C_{D,B}\right)_W = \frac{2r_b^2 \tan\gamma}{S\sqrt{\beta^2\tan^2\gamma - 1}}\,\alpha\left(\frac{\pi}{2} - \sin^{-1}\frac{1}{\beta\tan\gamma}\right) \tag{C7}$$

and utilizing the trigometric identity.

$$\frac{\pi}{2} - \sin^{-1}\frac{1}{\beta\tan\gamma} = \cos^{-1}\frac{1}{\beta\tan\gamma}$$

equation (C7) becomes

$$\left(C_{D,B}\right)_W = \frac{\left(2r_b^2\tan\gamma\right)\alpha}{S\sqrt{\beta^2\tan^2\gamma - 1}}\left(\cos^{-1}\frac{1}{\beta\tan\gamma}\right) \tag{C8}$$

and consequently, the expression for G is

$$G = \frac{2r_b^2\tan\gamma}{S\sqrt{\beta^2\tan^2\gamma - 1}}\cos^{-1}\frac{1}{\beta\tan\gamma} \tag{C9}$$

AN ANALYTICAL METHOD FOR PREDICTING LIFT AND DRAG CHARACTERISTICS OF FLAT-TOP WING-BODY COMBINATIONS AT SUPERSONIC SPEEDS

by

Dennis F. Hasson

ABSTRACT

An analysis was presented for predicting lift and drag characteristics of flat-top wing-body combinations at supersonic speeds. These combinations consist of a wing mounted above an expanding body with their apexes being coincident. The assumptions with which the analysis was made are the following:

1. The linear theory was applicable.
2. The leading edge of the wing was coincident or ahead of the body shock.
3. Condition of zero base drag (static pressure at the base equal to the stream static pressure).

The analysis was carried out by considering the individual terms which appear in the lift-drag relations separately, and utilizing the most recent theoretical methods to determine them. The analysis was applied to two flat-top wing-body combinations; namely, a semiconical body with an arrow planform wing, and a 3/4 power semibody with a diamond planform wing. For these combinations a free-stream Mach number of 3.35 satisfied the condition for the wing leading edge and the body bow shock to be coincident. To obtain a check on the analysis, the results were compared with experimental data at a Mach number of 3.35.